



HAL
open science

Switching From Subduction Zone Advance to Retreat Explains the Late Paleozoic Evolution of the East Junggar System, Central Asian Orogenic Belt

Yazhou Miao, Jian Zhang, Karel Schulmann, Alexandra Guy, Igor Soejono,
Yingde Jiang, Min Sun, Shuhui Zhang, Zhiyong Li

► **To cite this version:**

Yazhou Miao, Jian Zhang, Karel Schulmann, Alexandra Guy, Igor Soejono, et al.. Switching From Subduction Zone Advance to Retreat Explains the Late Paleozoic Evolution of the East Junggar System, Central Asian Orogenic Belt. *Tectonics*, 2024, 43, 10.1029/2024TC008254 . insu-04851360

HAL Id: insu-04851360

<https://insu.hal.science/insu-04851360v1>

Submitted on 20 Dec 2024

HAL is a multi-disciplinary open access archive for the deposit and dissemination of scientific research documents, whether they are published or not. The documents may come from teaching and research institutions in France or abroad, or from public or private research centers.

L'archive ouverte pluridisciplinaire **HAL**, est destinée au dépôt et à la diffusion de documents scientifiques de niveau recherche, publiés ou non, émanant des établissements d'enseignement et de recherche français ou étrangers, des laboratoires publics ou privés.

Copyright

Key Points:

- The Yemaquan arc and Dulate back-arc are affected by 310–280 Ma D₁ and 270–250 Ma D₂ events
- D₁ results from advancing mode of the Kalamaili subduction zone, and the closure of the Dulate back-arc basin
- D₂ results from the collisional reworking of the East Junggar system and indentation of Junggar promontory

Supporting Information:

Supporting Information may be found in the online version of this article.

Correspondence to:

J. Zhang and K. Schulmann,
jian@hku.hk;
karel.schulmann@geology.cz

Citation:

Miao, Y., Zhang, J., Schulmann, K., Guy, A., Soejono, I., Jiang, Y., et al. (2024). Switching from subduction zone advance to retreat explains the late Paleozoic evolution of the East Junggar system, Central Asian Orogenic Belt. *Tectonics*, 43, e2024TC008254. <https://doi.org/10.1029/2024TC008254>

Received 20 JAN 2024

Accepted 14 MAY 2024

Author Contributions:

Conceptualization: Jian Zhang

Data curation: Yazhou Miao, Karel Schulmann, Shuhui Zhang, Zhiyong Li

Formal analysis: Jian Zhang

Funding acquisition: Jian Zhang, Karel Schulmann, Yingde Jiang

Investigation: Yazhou Miao, Jian Zhang, Karel Schulmann, Shuhui Zhang, Zhiyong Li

Methodology: Jian Zhang

Project administration: Jian Zhang






Supervision: Jian Zhang

Writing – original draft: Yazhou Miao, Karel Schulmann, Alexandra Guy

Writing – review & editing:

Yazhou Miao, Jian Zhang, Karel Schulmann, Alexandra Guy, Igor Soejono, Yingde Jiang, Min Sun

Switching From Subduction Zone Advance to Retreat Explains the Late Paleozoic Evolution of the East Junggar System, Central Asian Orogenic Belt

Yazhou Miao^{1,2}, Jian Zhang² , Karel Schulmann^{1,3}, Alexandra Guy¹ , Igor Soejono¹, Yingde Jiang⁴ , Min Sun² , Shuhui Zhang⁵, and Zhiyong Li^{1,4} 

¹Czech Geological Survey, Praha, Czech Republic, ²Department of Earth Sciences, The University of Hong Kong, Hong Kong, China, ³Institut Terre et Environnement de Strasbourg, UMR 7063 Université de Strasbourg - CNRS, Strasbourg, France, ⁴State Key Laboratory of Isotope Geochemistry, Guangzhou Institute of Geochemistry, Chinese Academy of Sciences, Guangzhou, China, ⁵School of Earth Sciences and Engineering, Sun Yat-Sen University, Guangzhou, China

Abstract The geodynamic evolution of the East Junggar is examined by means of satellite imaging and field-based structural studies, U-Pb zircon geochronology and analysis of potential field geophysical data in the Yemaquan arc and the Dulate back-arc systems. The northern Yemaquan arc shows a pervasive WNW–ESE steep S₁ foliation that is related to the exhumation of Armantai ophiolitic mélange in an F₁ antiformal structure. The bedding of the Dulate sequences is folded by N–S-trending F₁ upright folds that are preserved in low strain domains. The timing of D₁ is estimated between 310 and 280 Ma. During D₂, previously folded Dulate sequences were orthogonally refolded by E–W-trending F₂ upright folds, resulting in Type-1 basin and dome interference pattern and pervasive E–W trending S₂ cleavage zones. The age of D₂ is constrained to be 270–250 Ma based on the dating of syn-tectonic pegmatites and deposition of syn-orogenic sedimentary rocks. The boundary between the Yemaquan arc and Dulate back-arc basin experienced reactivation through D₂ dextral transpressive shear zones. The D₁ fabrics are the consequence of the closure of the Dulate back-arc basin due to the advancing mode of Kalamaili subduction. Almost orthogonal Permian D₂ fabrics were generated by the N–S shortening of the East Junggar and the northward movement of the Junggar Block indenter. This D₂ deformation was associated with the anticlockwise rotation of the southern limb of the Mongolian Orocline, the scissor-like closure of the northerly Mongol–Okhotsk Ocean and the collision of the Mongolian and the Tarim–North China craton collages.

1. Introduction

The Central Asian Orogenic Belt (CAOB) is among the largest Phanerozoic accretionary orogenic belts in the world, characterized by subduction, accretion of arc systems, amalgamation of rigid Precambrian blocks and oroclinal bending (Şengör et al., 1993; Windley et al., 2007; Xiao et al., 2018). It has been recently interpreted as a supercollage consisting of three different collages: the Kazakhstan collage in the northwest, the Mongolian collage in the northeast and the Tarim–North China collage to the south (Xiao et al., 2015). The two northern collages in the CAOB are formed by large oroclinal systems named as the Kazakhstan and Mongolian oroclines. These oroclines are mutually separated by the crustal-scale Char-Erqis Zone (Figure 1; Windley et al., 2002, 2007; Xiao et al., 2015).

In the last decades, research on the CAOB has focused primarily on determining the subduction polarity and timing of closure of oceanic basins among various volcanic arcs (e.g., Geng et al., 2011; Wang et al., 2003; Wilhem et al., 2012). Little attention has been paid to the deformation features associated with the amalgamation of individual components forming the CAOB and the kinematics of late fault zones that disrupt the whole system (Choulet et al., 2016; Schulmann et al., 2023). For instance, previous studies in the West Junggar, which belongs to the Kazakhstan Orocline, have shown that the exhumation of mantle fragments was essentially linked to the regional-scale deformation associated with the amalgamation of individual tectonic units during the late Carboniferous (Choulet, Faure, et al., 2012; Zhang, Wang, Polat, Zhu, et al., 2018). These linear terranes in the CAOB, including arcs and accretionary wedges, were dissected and displaced by a series of major left-lateral (such as Erqis Fault) and right-lateral shear zones (such as Central Kazakhstan Fault) (Buslov et al., 2004; Hong et al., 2017; Laurent-Charvet et al., 2003; Li et al., 2017; Zhang et al., 2012). Available chronological data suggest that the fault zones were active in the Permian, possibly in response to the westward migration of the

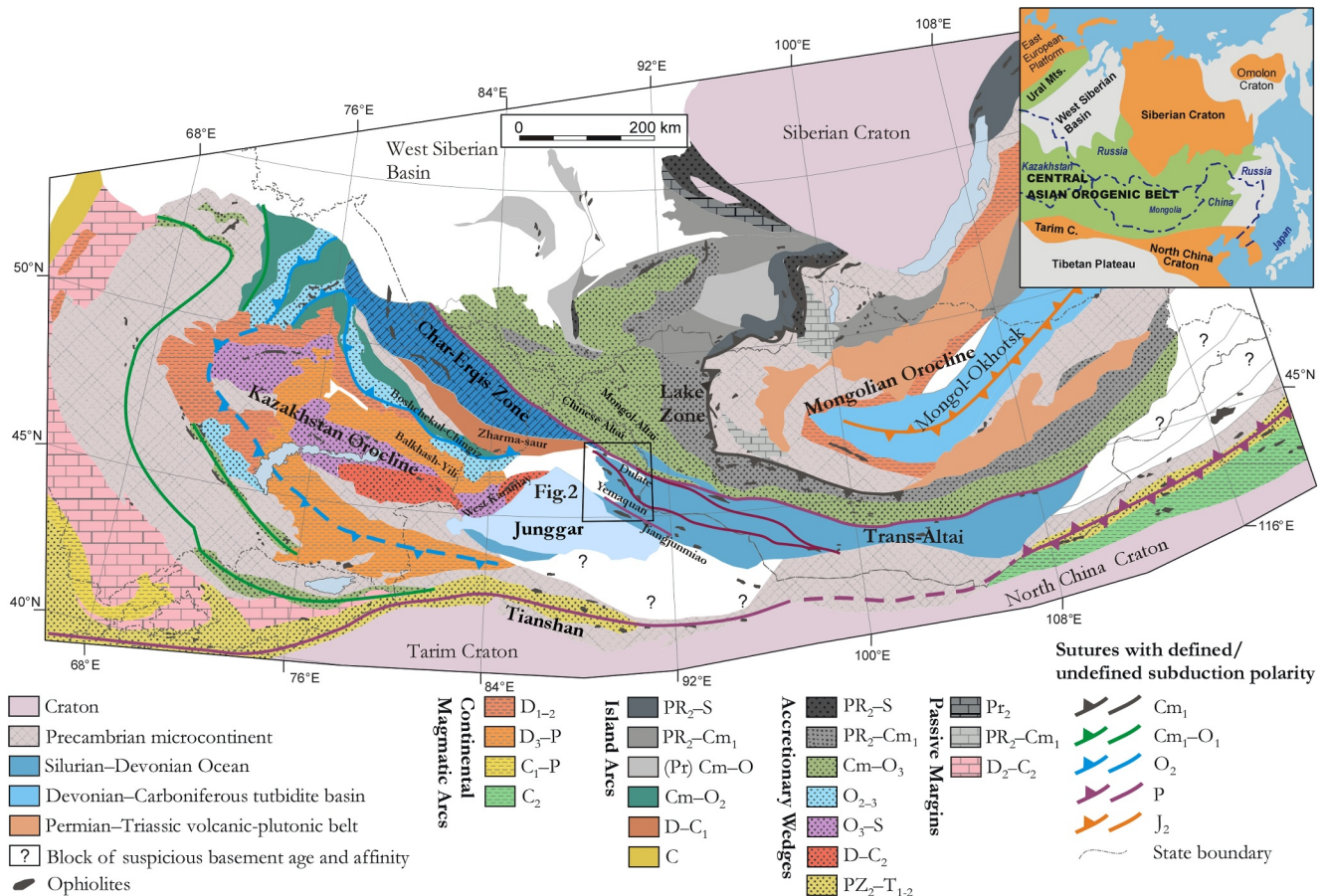


Figure 1. Simplified geological map of the Central Asian Orogenic Belt (revised after Guy et al., 2020).

Kazakhstan Orocline as a result of the convergence of the Siberian, Tarim and North China cratons (Li et al., 2017; Li, Sun, et al., 2015). However, the strike-slip shearing may also be caused by the indentation of a continental-sized rigid block into a weaker plastic crust, similar to the example of the India-Asian collision (Tapponnier et al., 1982, 2001). This hypothesis has been recently proposed for interpreting the indentation of the Junggar Block in the West Junggar (Miao, Zhang, Schulmann, Guy, et al., 2023).

In contrast to the West Junggar, which shows the activity of ENE–WSW-trending sinistral strike-slip zones (Choulet, Faure, et al., 2012; Miao, Zhang, Schulmann, Guy, et al., 2023; Zhang, Wang, Polat, Shen, et al., 2018), the East Junggar exhibits a series of WNW–ESE-trending strike-slip fault zones (Figure 1). These fault zones include the Armantai-Ulungur and Kalamaili fault zones, which contain ophiolitic mélanges of various age that are nearly parallel to the Erqis-Zaysan shear zone (Li et al., 2017; Li, He, et al., 2020; Li, Sun, et al., 2015). However, the exhumation of mantle rocks along these linear zones and the timing of large-scale strike-slip zones remain poorly constrained. Previous studies mainly focused on geochemical features of exhumed mantle rocks, which were interpreted as ophiolites accreted to elongated magmatic arcs (Xiao et al., 2008; Xiao et al., 2010; Yang et al., 2013; J. Zhang et al., 2018). However, it remains unclear whether the deformation history of the East Junggar reflects the same sequence of accretion and indentation process as that of the West Junggar.

To investigate the relationships between the East Junggar structural pattern, geometry of the Junggar Block and the activity of the Erqis-Zaysan Zone (EZZ), we carried out large-scale detailed structural mapping in the key areas of the Yemaquan arc and Dulute domain in the East Junggar (Zhaheba and Kalaan areas in Figure 2). We utilized available geophysical data, satellite images, and field-based structural analyses to constrain the succession of orogenic fabrics and finite strain pattern of the East Junggar. With the aid of U-Pb zircon geochronology and previously published U-Pb zircon ages, we established the timing of two major deformation events.

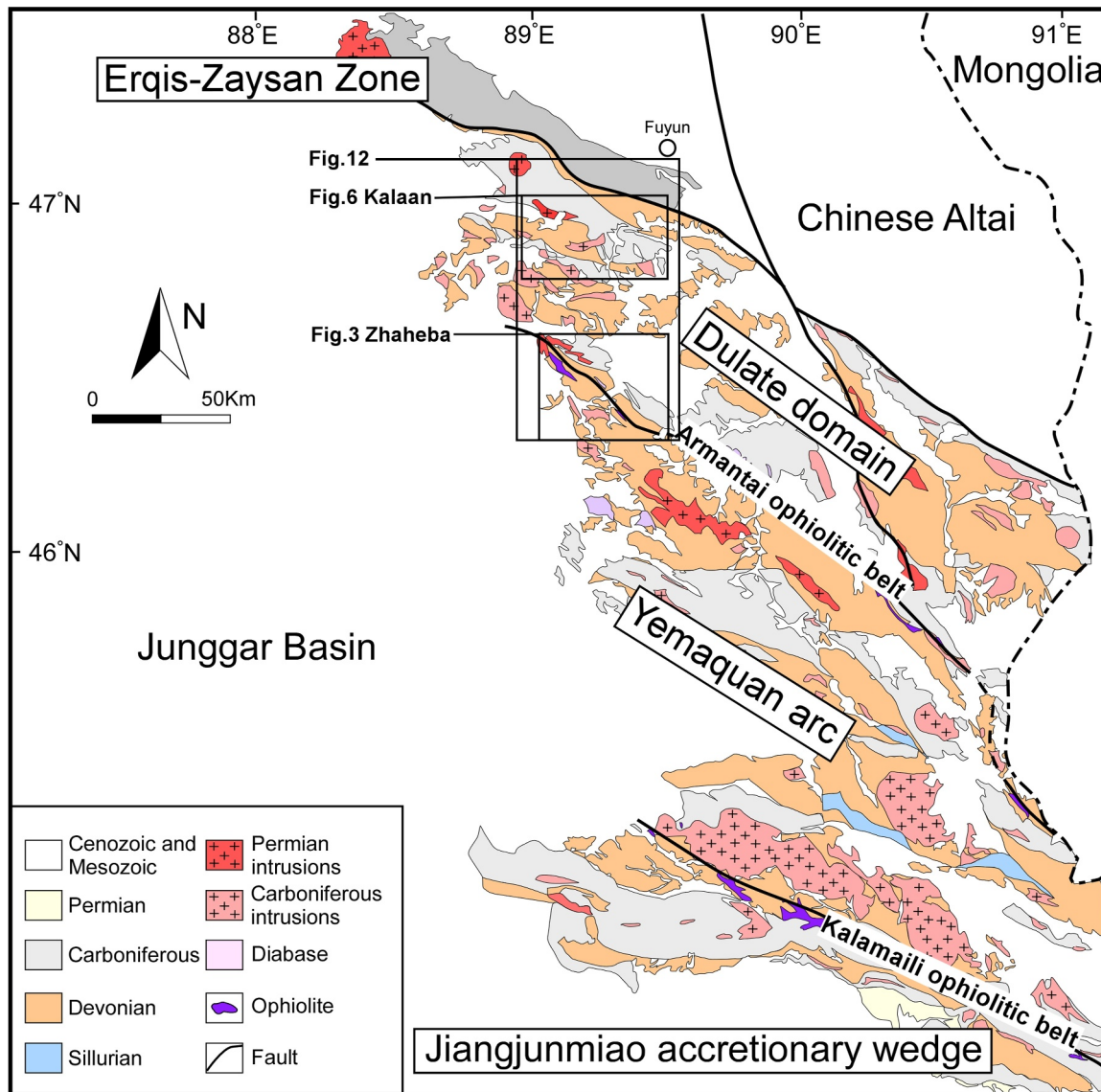


Figure 2. Simplified geological map of the East Junggar (revised after BGMRX, 1978).

These data provide crucial insights into the late Carboniferous–Permian polyphase shortening of the Carboniferous supra-subduction system, followed by indentation of the Junggar Block.

2. Geological Overview

The study area is located at the junction between the Kazakhstan and Mongolian Oroclines, to the south of the Char–Erqis zone (Figure 1). The northern limb of Kazakhstan Orocline occurs in the west and comprises Paleozoic volcanic–sedimentary sequences of the Zharma–Saur arc, Boshchekul–Chingiz arc, Toli unit, Mayile–Tangbale unit and West Karamay unit (Choulet, Cluzel, et al., 2012; Li et al., 2017). In the east part of the West Junggar exposures the Mesozoic–Cenozoic sedimentary rocks covering unknown basement of the Junggar Block (Zhou et al., 2018). Both the West Junggar and the Junggar Block are separated from the northerly Chinese Altai by the Char–Erqis Zone (the segment located in China is named the EZZ in this study) (Figure 1). East of the Junggar Block and south of the EZZ defines the East Junggar subduction system (Figure 2). This subduction system is further subdivided, from south to north, into the Jiangjunmiao accretionary complex, Yemaquan arc and Dulate domain, which are separated by the WNW–ESE–striking Kalamaili and Armantai ophiolitic mélanges,

respectively (Figure 2). These components were interpreted as part of a Devonian archipelago arc system that was successively amalgamated during the late Carboniferous within the Paleo-Asian Ocean (Xiao et al., 2009, 2010).

The southernmost part of the East Junggar is composed of the Jiangjunmiao accretionary complex with various rock types, including Devonian to Lower Carboniferous sandstone, mudstone, conglomerate, basalt, basaltic andesite, rhyolite, and tuff (Huang et al., 2018; Xiao et al., 2009; Zhang et al., 2021). The Devonian clastic sedimentary facies indicate a littoral-neritic environment (Cai et al., 2018; Zhang et al., 2013). The detrital zircon study of Zhang et al. (2013) indicates that these sedimentary rocks were deposited between 373 Ma and 345 Ma, implying a rapid orogenic uplift of the hanging-wall orogenic wedge (Zhang et al., 2013). The Jiangjunmiao accretionary complex was later unconformably covered by Upper Carboniferous (ca. 315 Ma) clastic sedimentary sequence that is interpreted to have formed as a forearc basin or slope sedimentary rocks (Huang et al., 2018). The U-Pb zircon ca. 314–306 Ma ages of rhyolites and geochemical features of basalts and rhyolites point to a post-orogenic extension event in the late Carboniferous. This extension is considered to be associated with the mantle upwelling of asthenospheric mantle (Su et al., 2012). The Kalamaili ophiolitic belt is mainly composed of Middle Devonian and Lower Carboniferous lava, tuff, chert, as well as abundant ultramafic and mafic igneous rocks, and mélanges (Liu et al., 2017; Long, Yuan, Sun, Xiao, et al., 2012). The LA-ICP-MS U-Pb zircon dating of diabase and overlying tuff in the Kalamaili ophiolitic belt revealed a range of dates (417–343 Ma) interpreted as the age of oceanic crust of the region (Huang et al., 2012). These data are consistent with the existence of late Devonian to early Carboniferous radiolarian fossils (Cai et al., 2018; Xu et al., 2020).

The Yemaquan arc is considered to have potentially developed on continental crust due to the Andean-type geochemistry signature from the Ordovician volcanic rocks and granite of the Tacheir tectonic window (Xu et al., 2013). The Paleozoic sedimentary sequence of the Yemaquan arc begins with a Silurian marine sedimentary succession that is interbedded with intermediate-felsic volcanic rocks (An et al., 2021). The overlying strata include Middle Devonian volcanic-clastic rocks, Lower Carboniferous volcanic, clastic, and carbonate rocks, as well as Upper Carboniferous siliciclastic and carbonate rocks (Long, Yuan, Sun, Xiao, et al., 2012; Xu et al., 2013).

The Armantai ophiolitic mélange, which extends from the Zhaheba area to the easterly China-Mongolia border, is mainly composed of serpentinites, serpentized peridotites, cumulate pyroxenites, and gabbros, troctolites, rodingites, diabases, basalts and cherts (Li et al., 2014; Luo et al., 2017). The SHRIMP U-Pb age of 495 Ma from plagiogranite and gabbro implies that the Armantai ophiolite may have been formed during the late Cambrian period (Liu et al., 2016; Zhang & Guo, 2010).

The Dulute domain consists of the Devonian–Carboniferous arc-related volcano-sedimentary sequences (Liu & Liu, 2014) that are intruded by late Paleozoic granitoids (e.g., Song et al., 2019; Tang et al., 2017). Therefore, this domain was traditionally believed to have formed in an intra-oceanic island arc setting during the late Paleozoic (Zhang et al., 2009). However, major and trace elements data and sedimentological features of the Carboniferous Nanmingshui Formation suggest that the volcanic-sedimentary succession of the Dulute domain may have developed in a back-arc basin setting (Tao et al., 2014). This assertion was confirmed by a recent sedimentological and detrital zircon study of the same region, which suggests that the Dulute domain represents a Carboniferous back-arc system separating the Yemaquan arc from the Chinese Altai accretionary wedge (Jiang et al., 2024).

3. Deformational History of the Zhaheba Area

3.1. Geology of the Zhaheba Area

The Zhaheba area covers a critical region that involves contact between various lithological units from the northern Yemaquan arc, Armantai ophiolitic mélange (or Zhaheba ophiolite) and southern Dulute back-arc domain (Figures 2 and 3a). The northern part of the Yemaquan arc is dominated by the Tuolanggekuduke Formation, which comprises pyroclastic rocks, minor limestone, and ferri-ferrous chert (Li et al., 2016; Zhang et al., 2009). This formation is unconformably overlain by the Kaxiweng and Jiangzierkuduke formations, which are dominated by volcanic tuff (Figure 3a; Li et al., 2014). The presence of adakites, Nb-enriched basalt, potassic basalts and peridotites collected from the Tuolanggekuduke Formation suggests a supra-subduction origin during the middle Devonian (Li et al., 2014; Xu et al., 2013).

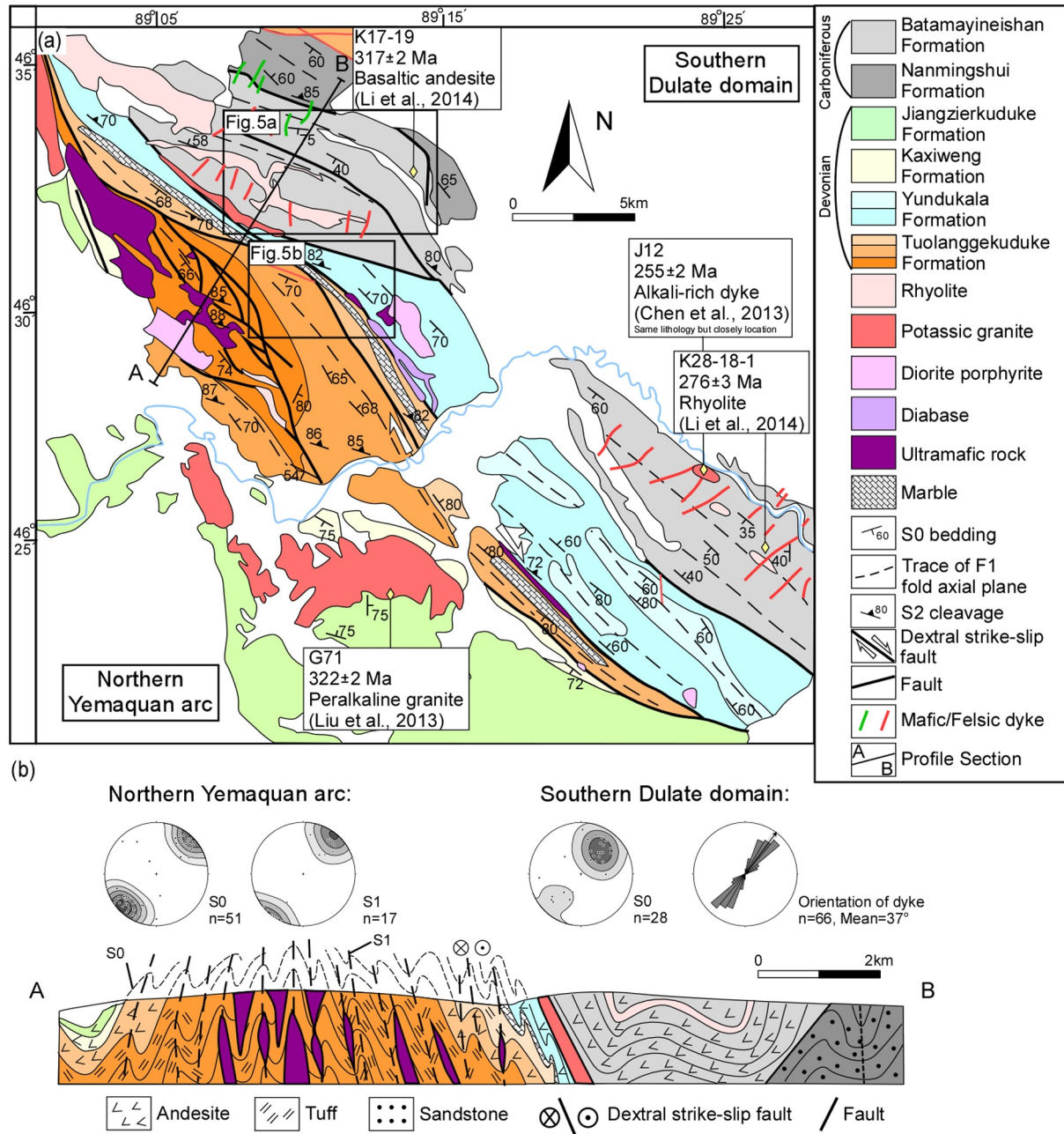


Figure 3. (a) The geological map of the Zhaheba area contains the northern Yemaquan arc and southern Dulute domain (basis of regional 1: 200,000 geological maps; BGMRX, 1978); (b) The interpretative cross-section for the Zhaheba area shows the primary structural features.

The Arantai ophiolitic mélangé is spatially associated with the Tuolanggekuduke Formation (Figure 2a). Compositions of chromium-bearing spinel from the serpentinites are similar to the MORB-type ophiolite, indicating that these rocks possibly represent residual asthenosphere mantle at a mid-ocean ridge (Ye et al., 2016). LA-ICP-MS U-Pb ages from the gabbro, diorite, and basalt from the ophiolite mélangé indicate that this oceanic crust formed between 495 Ma to 446 Ma (Luo et al., 2017). A ca. 322 Ma undeformed peralkaline A-type granite (Liu et al., 2013) intruded the Devonian Jiangzierkuduke and Kaxiweng formations to the south of the ophiolitic mélangé (Figure 3a).

In this study, the boundary between the Yemaquan arc and Dulute domain is marked by a NW–SE trending marble belt (Figure 3a). The southern part of the Dulute domain consists of three volcanic-sedimentary sequences. The

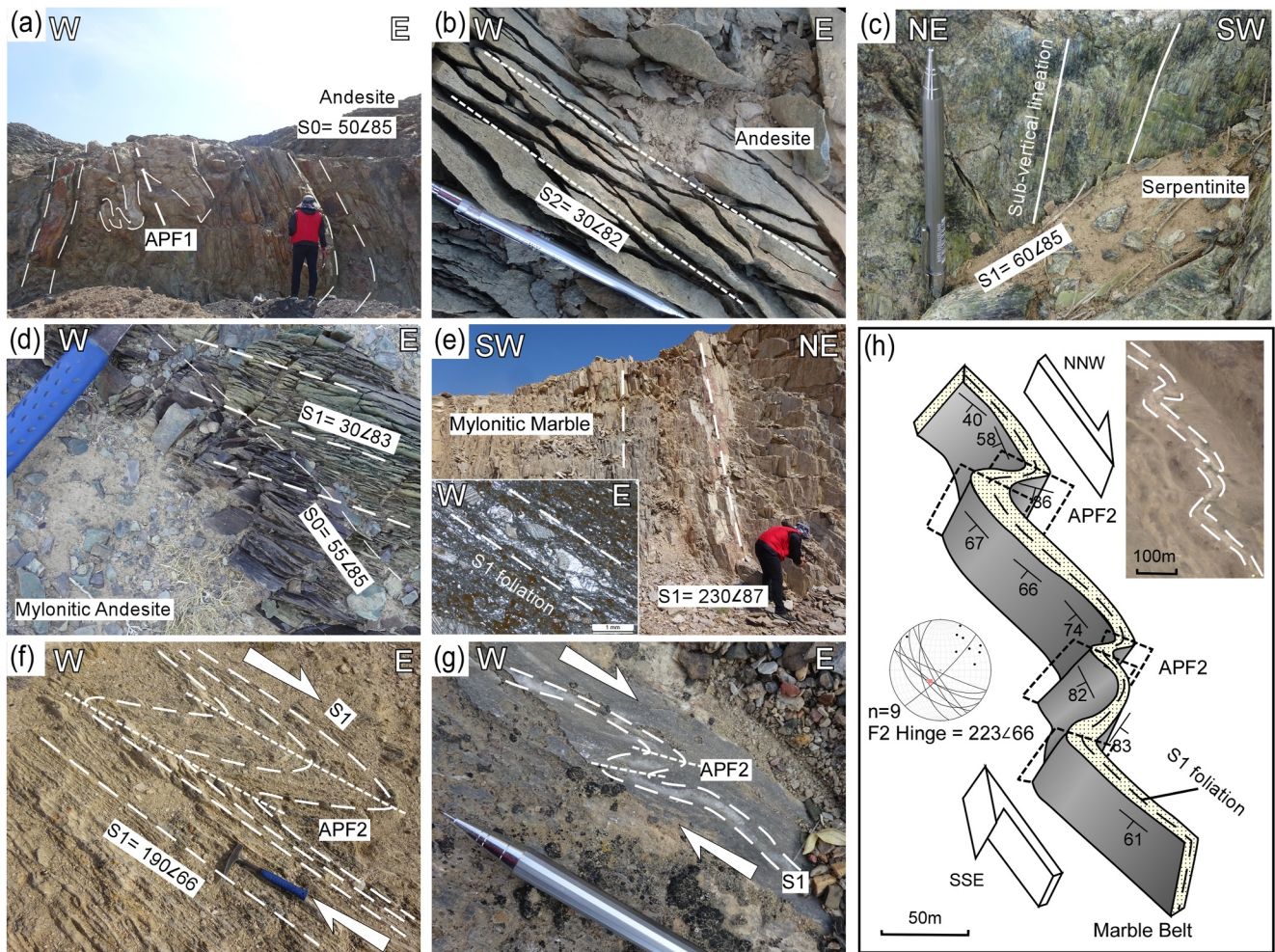


Figure 4. Field structural characteristic in the Zhaheba area; (a) Steep NW-SE trending S_0 bedding folded by upright folds F_1 ; (b) NW-SE-trending steep fracture S_2 cleavage; (c) Serpentinized peridotite lenses; (d) The S_0 bedding almost entirely transposed by greenschist facies S_1 cleavage; (e) A sub-vertical mylonitic marble belt; (f) Isoclinal F_2 folds in the mylonitic marble belt; (g) Mylonitic layers S_1 are subsequently folded by asymmetrical F_2 folds; (h) The S_1 marble mylonite belt is refolded by asymmetrical F_2 folds with E-W trending axial planes.

first sequence is the late Devonian to early Carboniferous Yundukala Formation, which consists mainly of shallow marine fine clastic rocks. The second sequence is the overlying Lower Carboniferous Nanmingshui Formation, which is composed essentially of sandstones and siltstones, while the Upper Carboniferous Batamayineishan Formation represents the third sequence that consists essentially of basalt and basaltic andesite. The Namingshui and Batamayineishan formations are intruded by numerous dolerite and Permian rhyolite dykes (Figure 3a). These dykes, together with a parallel set of tensional joints and thrusts, indicate a post-Carboniferous compressional deformation (Li et al., 2014).

3.2. Deformation Structures of the Zhaheba Area

Geological map and structural profile show NW-SE trending upright folding of stratification in the region, which is associated to the development of WNW-ESE-striking cleavage. These structures are also observed in the outcrops of the Armantai ophiolitic mélangé at the northern part of the Yemaquan arc (Figure 3). On the other hand, southern part of the Dulute domain exhibits mainly open upright folding of the Devonian and Carboniferous strata, characterized by wide synform with a core of the Batamayineishan Formation (Figure 3). Field observations from the Dulute domain show steep NW-SE trending S_0 bedding (Figure 4a) that is folded by F_1 upright folds with NW-SE sub-horizontal hinges (Figures 3b and 4a). The volcanics of the Nanmingshui Formation and volcanic-sedimentary rocks of the Yundukala Formation display a weak NW-trending ($N300^\circ$) steep fracture

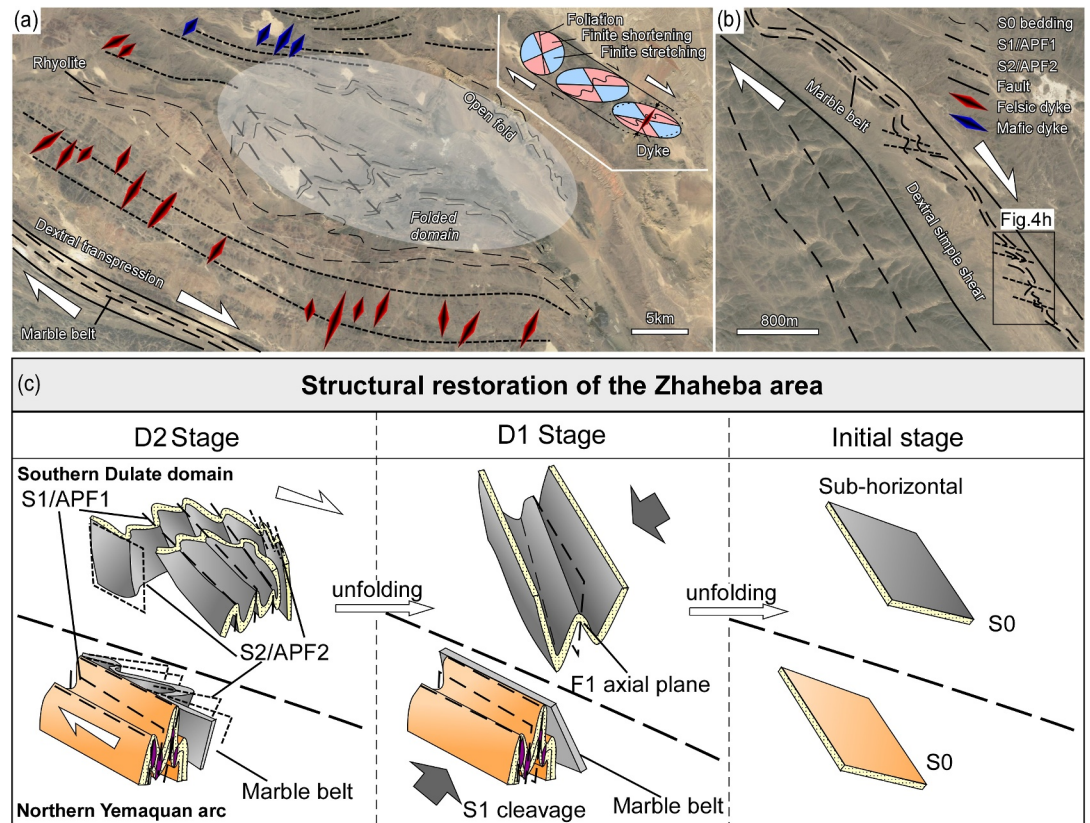


Figure 5. (a, b) The satellite image displays the asymmetric fold and the dextral strike-slip fault. (c) Structural restoration of the Zhaheba area.

cleavage (Figure 4b). Both the bedding and cleavage are crosscut by sub-vertical N37° trending dolerite and rhyolite dykes (Figure 3b).

In the northern part of the Yemaquan arc, the serpentinized peridotite lenses of the Armantai ophiolitic mélangé show low grade sub-vertical N330–340° trending S1 foliation, bearing a sub-vertical stretching lineation defined by serpentine minerals (Figures 3 and 4c). The volcanic-sedimentary strata of the surrounding Devonian Tuolanggekuduke Formation are deformed by F₁ upright folds with sub-horizontal hinges. The bedding becomes almost entirely transposed by greenschist facies cleavage S₁, which is oriented at variable angles to bedding S₀ (Figures 3 and 4d). In general, the structural pattern of the northern Yemaquan arc shows dome-like structure cored by serpentinite and gabbroic lenses, which are associated with close-to-isoclinal upright folding of the host Devonian sequences and transposition of S₀ bedding by S₁ cleavage (Figure 3b).

A sub-vertical mylonitic marble belt marks an important tectonic boundary between the northern part of Yemaquan arc structure and the southern Dulute domain (Figure 4d). The bedding of the mylonitic marble has been entirely transposed by sub-vertical foliation S₁ (Figure 4e). The marble S₁ microstructure is characterized by dynamic recrystallization, leading to the development of fine-grained matrix surrounding large clasts of twinned calcite (inset in Figure 4e). The nature of the thick and straight twins in the calcite clasts indicate a temperature of deformation consistent with a temperature range 150–300°C (Burkhard, 1990; Passchier & Trouw, 2005). In some places, marble mylonitic layers S₁ are subsequently folded by asymmetrical F₂ folds of varying sizes (Figures 4f and 4g), as also apparent from the right inset of Figure 4h.

The analysis of the satellite imagery reveals the deformation of the mylonitic marble belt, providing further support for the idea of dextral shearing at the boundary between the Yemaquan arc and the Dulute domain (Figure 5b). The S₁ marble mylonite belt is refolded by asymmetrical F₂ folds with E–W trending axial planes (Figure 4h). The long limbs of these F₂ asymmetrical folds dip steeply to the NE and the short limbs dip to the NW, indicating that dextral shear has affected the steeply NE dipping S₁ fabric (Figure 4h).

The satellite imagery further reveals a detailed structural pattern of the southern Dulute domain sequences, which is in the northern mylonitic marble belt (Figure 5a). In this image, the volcanic and sedimentary bedding is folded by upright, open to close, symmetrical to weakly asymmetrical F_1 folds with NW–SE-trending axial planes. The region south of the folded domain is characterized by bedding and fracture cleavage oriented at ca. 40° to axial planes of F_1 folds. This cleavage zone is parallelized with the mylonitic marble belt and crosscut by a series of dolerite and rhyolite dykes perpendicular to it. The NW margin of folded domain shows presence of open folds affecting the bedding with generally N to NNE trending axial planes. Further to the NW, there occurs a zone of bedding parallel to NW–SE trending fracture cleavage that is again crosscut by mafic and felsic dykes at right angle.

3.3. Restoration of the Superposed Folding Pattern

Combining the field structural data with the satellite imagery (Figures 4 and 5) allows the restoration of the finite strain pattern in both northern Yemaquan arc and southern Dulute domain (Figure 5c). The former region shows a two-stage evolution characterized by: (a) the formation of an antiformal structure cored by serpentinite, where bedding of the Devonian formations was reworked by greenschist facies S_1 cleavage during the D_1 stage, and (b) this fabric was later reworked by dextral D_2 shearing developed along the NE limb of the D_1 domal structure. This major mylonitic marble shear zone represents a major tectonic boundary between the Yemaquan arc and Dulute domain.

The southern Dulute domain also experienced two-stage structural evolution. The first event can be depicted in the satellite imagery and is marked by relics of upright folds with NW–SE trending axial planes. Close symmetrical folds are only preserved in the central part of the synform composed of the Batamaynesihan Formation (Figures 3a and 5a). The synform is surrounded by the older Nanmingshui Formation in the north and the Yundukala Formation in the south, both of which show uniformly $N30^\circ$ dipping beds (Figure 3b), and the development of bedding parallel fracture cleavage (Figure 4b), which is crosscut by dolerite and rhyolite dykes. In addition, the open folds in the NE part of synform core show axial planes that deviate from those of the central part of the synform. We interpret these folds in the synform core as a region preserving relics of F_1 upright folds, whereas the open folds at the NE margin of the synform show effects of unfolding of these folds during the D_2 shortening event (inset in Figure 5a). The D_2 deformation prevails in regions close to the marble belt (Figure 5b) and to the north region where the fracture cleavage S_2 developed. The synform thus represent a low strain domain where D_1 structures are preserved from ubiquitous D_2 reworking. In NE termination of this low strain domain, the D_2 deformation further amplifies the F_1 folds while on its NE flank it unfolds them as the limb region of large F_1 synform rotate into the direction of maximum D_2 stretching (Ramsay, 1962, 1967; inset in Figure 5a). The dolerite and rhyolite dykes crosscut the regions experiencing strong D_2 shortening and represent tensional fractures oriented parallel to the maximum compressive D_2 stress (inset in Figure 5a).

4. Deformational History of the Kalaan Area

4.1. Geology of the Kalaan Area

The Kalaan area is located in the northern Dulute domain that is directly adjacent to the EZZ (Figures 2 and 6a). The strata of this region consist of Devonian to Carboniferous volcanic-sedimentary rocks. The geochemical characteristics of the volcanic rocks suggest that they formed in an island-arc setting (Yang et al., 2012; Zhang et al., 2009). The Lower Carboniferous Heishantou Formation, mainly preserved in the northern part, comprises andesite, tuff, and sandstone. The Nanmingshui Formation mainly consists of two lithologic end-members: from the bottom to the top, these are shallow water marine-terrestrial sedimentary sequences and littoral shallow water marine sequences. The Haerjiawu Formation was deposited unconformably above the older sedimentary strata (Figure 6a). Permian strata are rarely exposed in this domain and are characterized by sub-vertical bedding.

Carboniferous (ca. 330 Ma) and Permian (ca. 280–270 Ma) magmatic intrusions and dykes are widely exposed in the area (Liu et al., 2019; this study). The granitoid plutons and dykes are represented by biotite monzogranite, monzogranite, quartz porphyry, dioritic porphyrite, and diorite (Liu et al., 2019). They are commonly in the form of sheets that are either oriented in the NW–SE direction or folded during later deformation (Figure 6a).

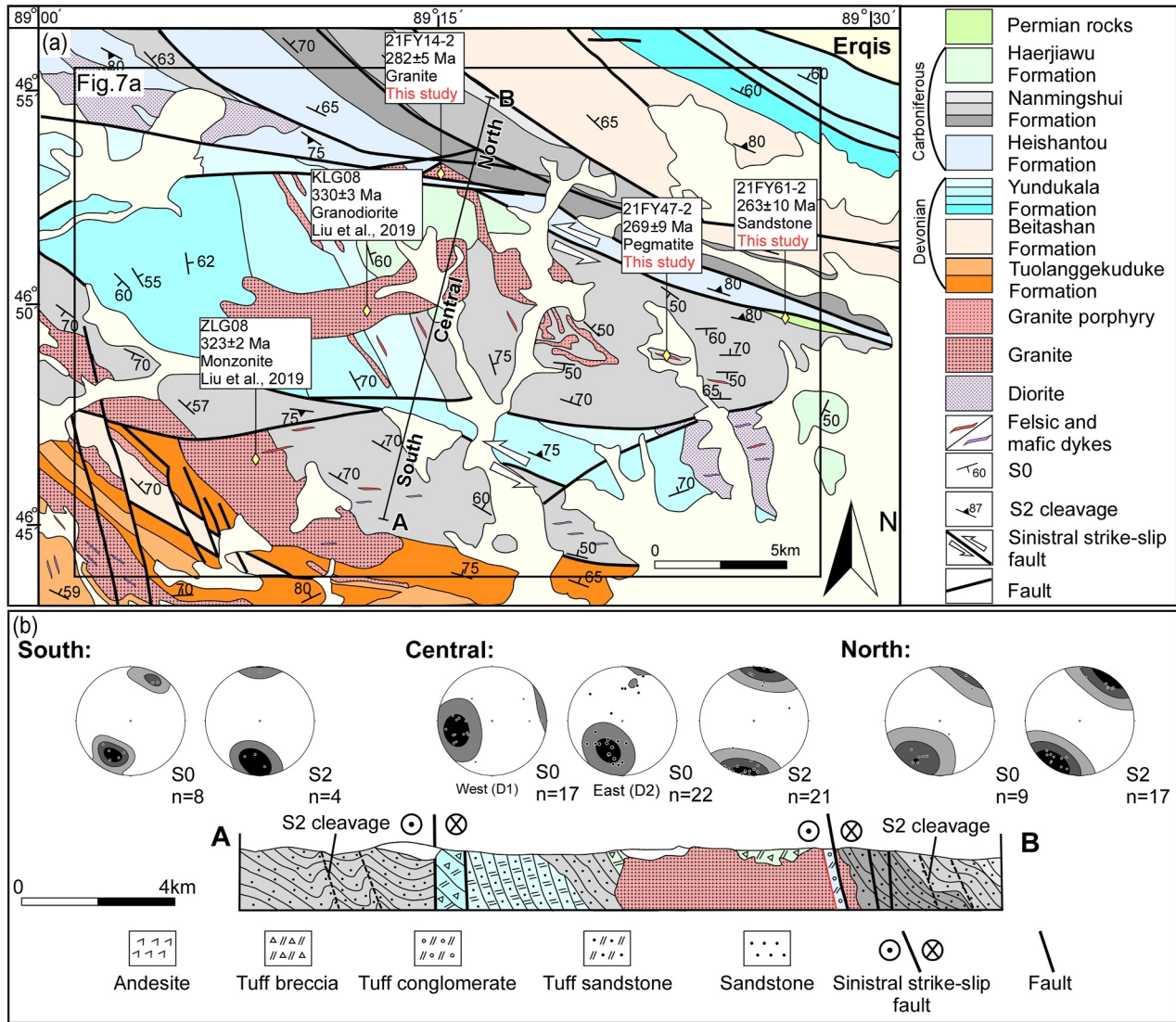


Figure 6. (a) The geological map of the Kalaan area, located in the northern Dulute domain and adjacent to the Erqis-Zaysan zone (basis of regional 1: 200,000 geological maps; BGMRX, 1978); (b) The interpretative cross-section for the Kalaan area shows the primary structural features.

4.2. Deformation Structures of the Kalaan Area

The southern part of the Kalaan area mainly consists of the Devonian Tuolanggekuduke and the Carboniferous Nanmingshui Formations. The central sector consists of the Devonian Yundukala and the Carboniferous Nanmingshui Formations. The northern part of the studied area is characterized by the Carboniferous sequences of Heishantou and Nanmingshui Formations (Figure 6a). All the formations mainly exhibit WNW–ESE structural trends (Figure 6b).

Two deformation events have been identified in the studied area: (a) the earliest D_1 deformation can be observed mainly in the western part of the central sector (Figure 6a). It is characterized by the $N350^\circ$ trending folds with sub-vertical eastwards or westwards dipping S_0 , which is defined by the alternations of competent sandstone and incompetent siltstones (Figure 7e). Although S_1 cleavage was not observed, the distribution of bedding poles in the stereonets (Figure 6b) indicates that the originally horizontal bedding was folded by upright F_1 folds with sub-horizontal hinges. (b) The D_2 deformation heterogeneously affected variably dipping S_0 and reoriented them to $N310$ – 290° trending (Figure 7d). Toward the east, the previously verticalized $N350^\circ$ trending S_0 was refolded by a new set of almost E–W-trending upright F_2 folds. As a result of this folding, the S_0 were rotated to the NW–SE direction and dip either to the NE or SW (Figure 6b). In some places, the F_2 folds affect the upright F_1 folds,

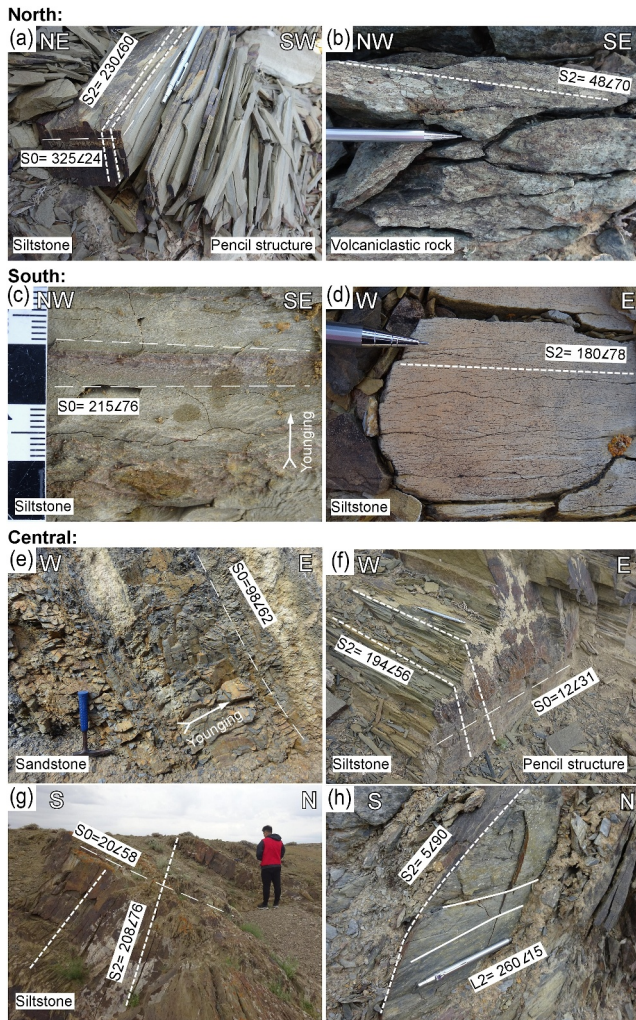


Figure 7. Field structural characteristic in the Kalaan area; (a–d) The sub-horizontal S_0 was cross-cut by NWW–SEE trending S_2 cleavage; (e) Photographs of volcanic-sedimentary which is characterized by the alternations of competent sandstone beds and incompetent siltstones; (f) Widely distributed pencil structure; (g) The S_0 bedding was transposed by almost E–W trending S_2 axial plane cleavage; (h) Shallowly plunging lineation L_2 .

generating the Type 1 (basins and domes) interference fold pattern (Ramsay, 1962), which is clearly shown on the satellite imagery (Figure 8d).

In the eastern part of the central sector, the intensity of D_2 deformation gradually increases, resulting in intense folding of S_0 by the tight upright F_2 folds (Figure 8d). The intersection of S_0 bedding and S_2 forms characteristic and widely distributed pencil structure (Figure 7f), while S_0 becomes transposed by almost E–W trending S_2 axial plane cleavage that bears shallowly plunging lineation L_2 (Figures 7g and 7h). Both the northern and southern parts of the study area show a similar structural pattern, marked by the nearly complete transposition of S_0 (Figures 7a and 7c) by the WNW–ESE-trending slaty cleavage (Figures 7b and 7d). In the same area, the volcanic-clastic rocks display a higher finite strain state, as manifested by the strong elongation of pumice lapilli (Figure 7b).

Satellite imagery allows a clearer visualization of the D_1 and D_2 structural pattern (Figure 8a). The S_1 fabric is well preserved in the western portion of the study area. The D_1 fabrics in the north are rotated to the NW–SE direction whereas in the south the degree of transposition is very high. The central sector shows well preserved $N340$ – 330° orientation of steeply dipping beddings as a result of F_1 upright folding (Figure 8d). This sector represents a low strain domain, where the D_1 structural grain is well preserved (Figure 8a). Toward the east, early structures experienced significant D_2 shortening, resulting in an interference fold pattern that is well marked by the folded granitic dykes (Figure 8d). Further east, the intensity of D_2 increases, leading to the obliteration of the D_1 fabrics. The high degree of D_2 transposition is clearly visible in the southern and northern parts of the studied section (Figures 8b and 8c).

4.3. Restoration of the Superposed Folding Pattern

Based on the structural mapping and satellite imagery, the temporal and spatial relations between D_1 and D_2 can be restored (Figure 8e). This restoration shows that the original horizontal disposition of the Devonian and Carboniferous strata were folded by NNW–SSE trending F_1 upright folds with sub-horizontal hinges (Figure 8e). The D_2 deformation resulted in the formation of almost E–W-trending upright F_2 folds that folded variously dipping S_0 . In the central sector of the study area, F_2 folding resulted in the development of Type 1 basin and dome interference fold pattern (Ramsay, 1962), in the north, east and south sectors the F_2 folds entirely transposed the all previous structures. Therefore, the central sector can be regarded as a low strain domain or megalithon, where the D_1 fabrics are partly preserved whereas the surrounding areas are dominated by high strain zones of regional D_2 deformation.

5. Geochronology Constraints: Zircon U-Pb Geochronology

To constrain the timing of the D_1 – D_2 deformations, we collected three representative samples of different rock types from the Kalaan area. We utilized LA-ICP-MS to carry out high-precision U-Pb zircon age dating. Unfortunately, we were unable to obtain suitable samples for the Zhaheba area, so the structural history of the area was constrained using previously reported geochronological data. The sample description and age results are listed in Table S1.

5.1. Sandstone 21FY61-2

The sandstone Sample 21FY61-2 was collected from the eastern part of the central sector in the Kalaan area (Figure 5a) and was used to constrain the depositional age of the deformed sedimentary rocks. In the field, the sandstone exhibits sub-vertical WNW–ESE-trending bedding (Figure 9a) that is defined by the lithic fragment

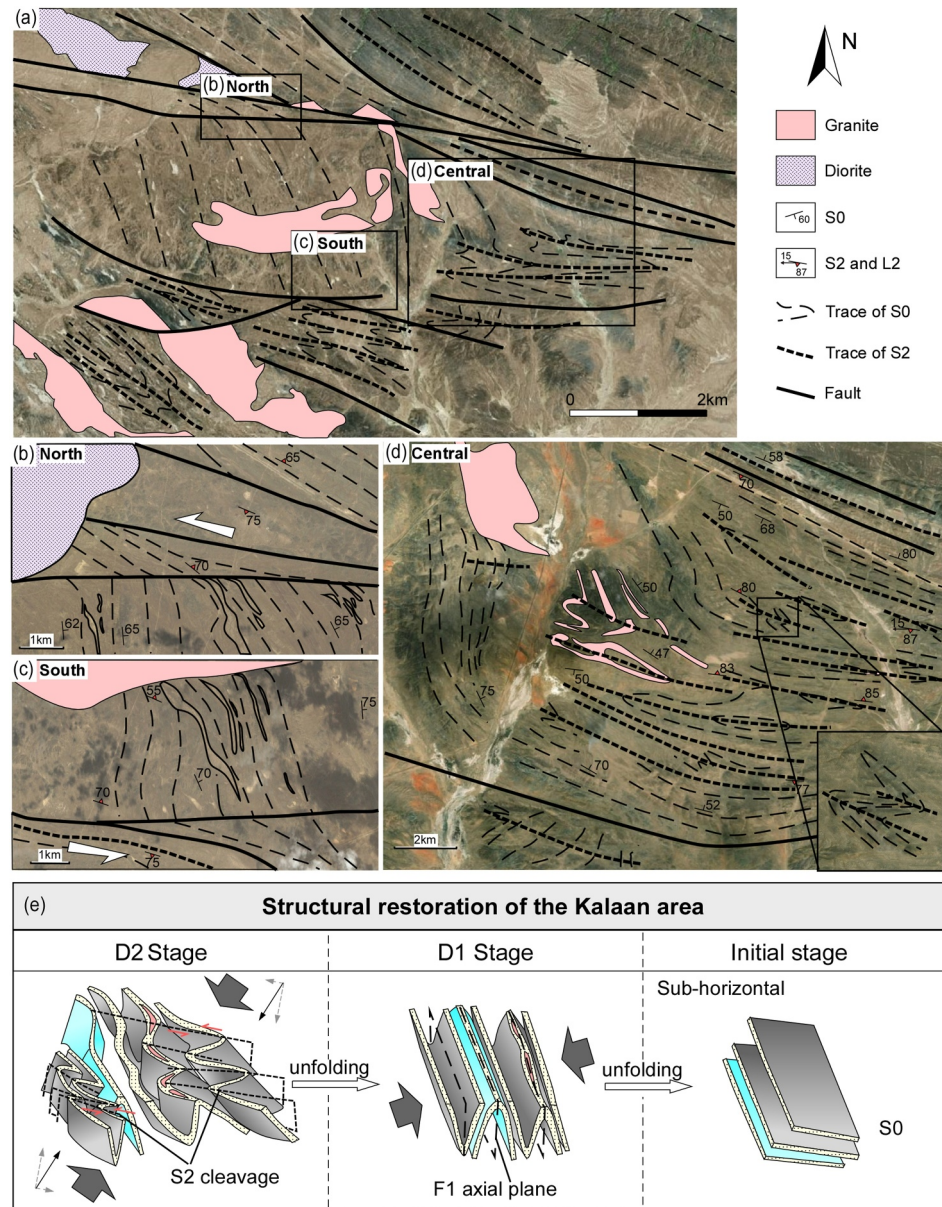


Figure 8. (a) The satellite image of the Kalaan area; (b–d) The satellite image and structural characteristics of the north and south part around the central sector; (e) Structural restoration of the Kalaan area.

and matrix under the microscope (Figure 9b). The presence of angular quartz grains in the sandstone indicates the supply of sediments from the proximal source regions (Figure 9b). Zircon grains extracted from Sample 21FY61-2 are mostly prismatic and subhedral in shape, with length ranging from 60 to 100 μm and aspect ratio of 1:1–2:1 (Figure 10a), indicating an igneous origin. In addition, CL images of zircon also show a typical oscillatory zoning and a magmatic origin (Figure 10b), which is consistent with the Th/U ratio of 0.10–0.80 (Table S1). U–Pb zircon dating of 42 zircons yielded ages between ca. 700 and 250 Ma (Figures 10a and 10b). The maximum depositional age of 263 ± 10 Ma is determined by using the $^{206}\text{Pb}/^{238}\text{U}$ weighted mean age from the four youngest analyses (Figure 10a). This sandstone shows an older zircon age peaks at ca. 317 Ma, which implies that the detritus was transported from a proximal source.

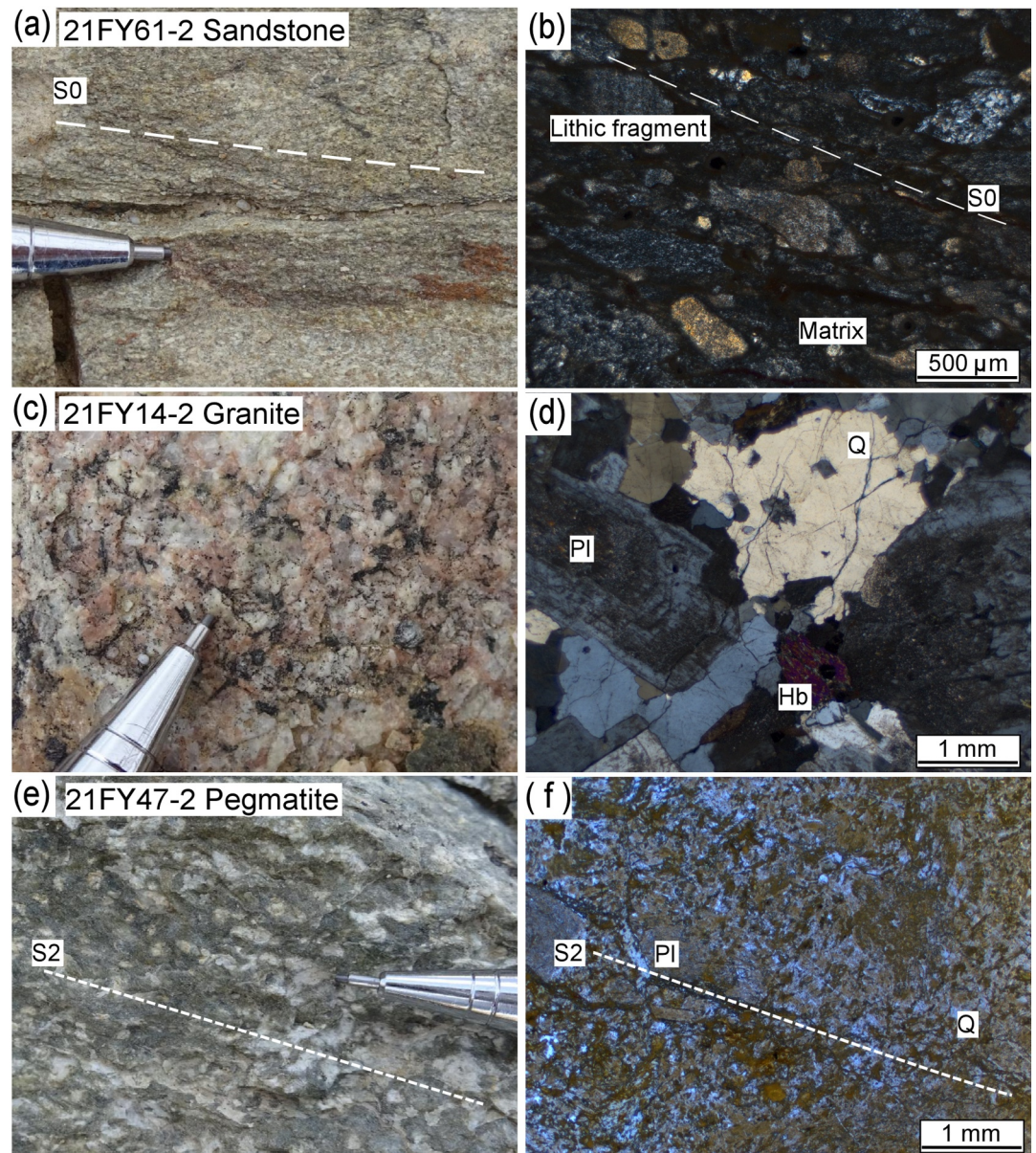


Figure 9. Representative photos of the selected samples and micro-photography of the samples chosen for U-Pb zircon dating.

5.2. Granite 21FY14-2

The granite Sample 21FY14-2 was collected from an undeformed granite intrusion in the central domain of the Kalaan area (Figures 5a and 9c). In the field, the granite pluton clearly intrudes and truncates the major D_1 fabric, but it is dissected by the WNW–ESE-trending fault (Figure 5a). Under the microscope, the granite displays a typical granitic texture characterized by the euhedral plagioclase, subhedral quartz and minor hornblende (Figure 9d). Zircon grains from the sample have length of 50–200 μm and display euhedral to subhedral crystal shapes with sharp or rounded terminations. CL images are characterized by oscillatory zoning texture and indicate a magmatic origin (Figure 10c). Th/U ratio varies from 0.44 to 1.02 (Table S1). A total of 12 analyzed spots gave a $^{206}\text{Pb}/^{238}\text{U}$ weighted mean age of 282 ± 5 Ma (Figure 10c), which is interpreted as the crystallization age of the granitic intrusion.

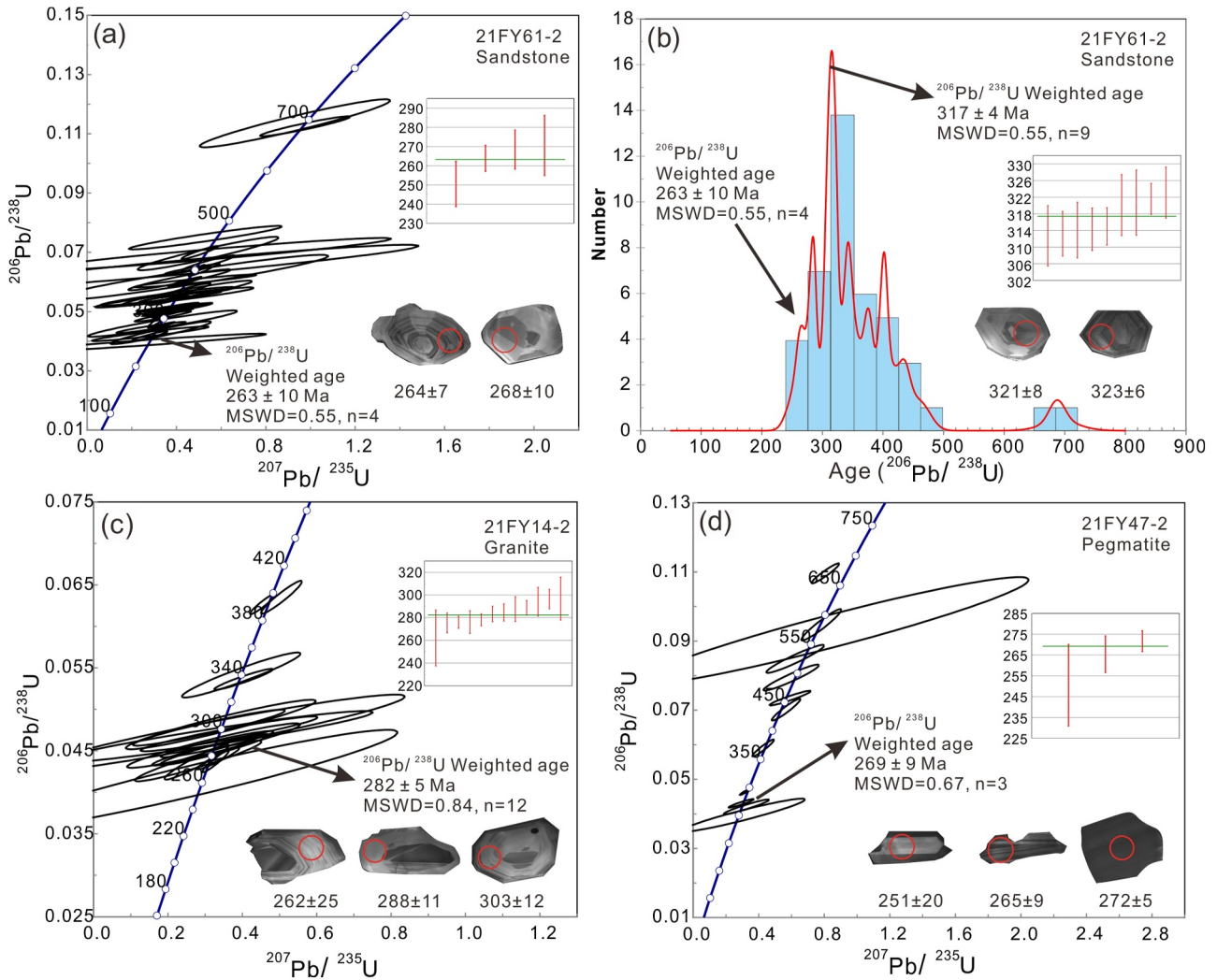


Figure 10. The CL images of zircons from samples and Concordia diagrams of LA-ICP-MS U-Pb zircon analytical results.

5.3. Pegmatite 21FY47-2

Sample 21FY47-2 was collected from granite–pegmatite dykes that trend WNW–ESE in the eastern part of the central domain of the Kalaan area (Figure 5a). In the field, these pegmatite dykes are emplaced parallel to the axial plane of the F_2 folds (Figure 5a) and develop penetrative S_2 foliations (Figure 9e). In the thin section, the sample contains fine-grained quartz and plagioclase (Figure 9f). Zircon grains are stubby to prismatic in crystal shape that generally have length of 50–100 μm with aspect ratio ranging from 1:1 to 2:1. The CL images exhibit blurred oscillatory or lath-shaped zoning without obvious inherited cores, indicative of magmatic origin (Figure 10d). The zircon grains show high Th/U ratio of 0.28–0.93 (Table S1). A total of 12 analyses were obtained from the sample, of which three youngest analyses yield a $^{206}\text{Pb}/^{238}\text{U}$ weighted mean age of 269 ± 9 Ma (Figure 10d). This age represents the crystallization age of these dykes, indicating their emplacement during the D_2 deformation. The remaining nine older zircon analyses vary in age from 670 Ma to 292 Ma and are interpreted as xenocrysts derived from the melting of a sedimentary source.

6. Magnetic and Gravity Analysis of the East Junggar Crustal Structures

The magnetic and gravity anomalies are examined to characterize the crustal structures with various signal treatments, and to analyze the distribution of the geophysical fabrics with the lineament extraction at the junction among the East Junggar, the Chinese Altai and the Junggar Block (Figure 11). This method allows the

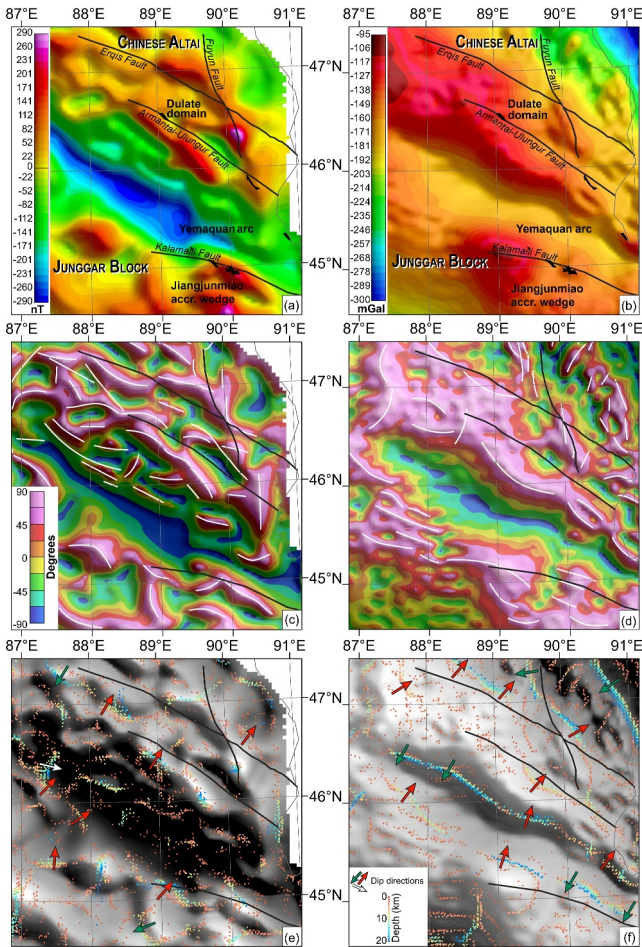


Figure 11. Major crustal structures constrained by magnetic and gravity signal analyses. The boundaries of the different units, the principal faults and the ophiolites described in this study are superimposed on each map. (a) Magnetic map extracted from the Earth Magnetic Anomaly Grid available at a spatial resolution of 2×2 arc min. (b) Bouguer gravity anomaly map extracted from the Earth Global Model 08 available at a spatial resolution of 2.5×2.5 arc min. (c) Tilt angle of the magnetic anomalies and the main lineaments (white lines). (d) Tilt angle of the gravity anomalies and the main lineaments (white lines). (e) Multiscale edge analysis from the surface to 20 km depth of the analytic signal results computed from the magnetic anomaly map in gray scale. (f) Multiscale edge analysis from the surface to 20 km depth of the gravity results computed from the Bouguer gravity map.

main NW–SE oriented faults (Erqis, Arantai-Ulungur and Kalamaili faults); (b) the NE–SW-trending lineaments are located in the Chinese Altai, the eastern part of the Dulute domain and the northwestern part of the Yemaquan arc; and (c) the N–S-trending lineaments are sub-parallel to the Fuyun fault and densely distributed around its trace.

The magnetic and gravity lineament maps also exhibit a 300 km long and 40 km wide NW–SE-trending area in the center of the Yemaquan arc to the Junggar Block that lack evidence for any significant lineaments.

6.3. Multiscale Edge Analysis—Distribution and Orientation of the Main Tectonic Contacts

After calculating the analytic signal of the magnetic anomalies and the Bouguer gravity anomalies, the multiscale edge detection is computed for 20 upward continuations from 0 to 40 km (Archibald et al., 1999; Holden et al., 2000; Hornby et al., 1999; Vallée et al., 2004). This method provides insights concerning the locations and

quantification of anomaly trends and their correlation with the lithologies, and thus, enables the structural analysis of orogenic fabrics (details methodology refers to Guy et al., 2020 and references therein).

6.1. Magnetic and Gravity Anomaly Maps

The magnetic data are available at a spatial resolution of 2×2 arc min from the Earth Magnetic Anomaly Grid (Maus et al., 2009). The East Junggar magnetic anomalies were reduced to the north magnetic pole using 66.1° for inclination and 3° for declination and the magnitude of the regional field of 57,383 nT according to the International Geomagnetic Reference Field. The resulting grid ranges from -290 to 290 nT (Figure 11a). Important magnetic anomalies were depicted in the Junggar Block, the Dulute domain and the Yemaquan arc, and the Jiangjunmiao accretionary wedge. The central part of the Yemaquan arc mostly corresponds to a 120 km long-wavelength magnetic low except for its contact with the Dulute domain. The ophiolitic mélanges of the Arantai ophiolitic belt coincide with moderate magnetic highs, whereas a prominent magnetic high correlates with the Kalamaili ophiolitic belt. The Arantai-Ulungur fault is not accurately defined by the magnetic gradient, which is located more to the south. A similar observation can be made for the Kalamaili fault.

The Bouguer gravity data are available at a spatial resolution of 2.5×2.5 arc min from the Earth Global Model 08 (Pavlis et al., 2012). The East Junggar Bouguer gravity anomalies range from -300 to -95 mGal (Figure 11b). Two NW–SE-trending approximately 100 km long-wavelength gravity highs can be observed: one extended across the EZZ to the Dulute domain and the northern part of the Yemaquan arc, the second straddling the Kalamaili ophiolitic belt. They include the ophiolitic belts. The central part of the Yemaquan arc and the Junggar Block correspond to an intermediate gravity signal. The gravity low is observed at the northeastern part of the Chinese Altai and corresponds to the Mongol-Altai accretionary wedge. The Arantai-Ulungur and Kalamaili fault zones do not correlate with strong localized gravity gradients.

6.2. Tilt Angle—Geophysical Mapping of the Main Structural Fabrics

The tilt angle, calculated on both magnetic and Bouguer gravity anomalies, allows the correlation between the main tectonic fabrics of the basement and the extracted geophysical lineaments (Miller & Singh, 1994; Verduzco et al., 2004). Three groups of magnetic and gravity lineaments can be distinguished (Figures 11c and 11d): (a) the WNW–ESE-trending lineaments are the most numerous and distributed from the Chinese Altai to the East Junggar and the Junggar Block. These lineaments are sub-parallel to the three

dips of major geological contacts from 0 to 20 km depth (Figures 11e and 11f). The magnetic and gravity multiscale edge results exhibit NE-dipping contacts (Red arrows in Figures 11e and 11f), which are equally distributed in the Chinese Altai and the East Junggar. These contacts find their counterparts in the SW-dipping contacts (Green arrows). Both types of contacts belong to the NW–SE-oriented geophysical lineaments. One ESE-dipping contact is observed on the magnetic map at the assumed border between the Junggar Block and the Yemaquan arc.

7. Discussion

7.1. Timing Constraints on the Regional D₁ and D₂ Deformations

In the Zhaheba area, the Devonian–Carboniferous sequences experienced both D₁ and D₂ deformations (Figure 5c). The maximum age of the D₁ deformation is constrained by the youngest zircon age of 276 ± 3 Ma from the rhyolite collected from the Batamayineishan Formation (Li et al., 2014). The end of the D₂ deformation is determined by the age of a trachyte porphyry dyke (255 ± 2 Ma) that intrudes pyroxene andesitic porphyrite of the Batamayineishan Formation (Chen et al., 2013). This dyke is oriented in NW–SE direction, almost parallel to the Permian cleavage and the Armantai–Ulungur fault zone. Based on the above age constraints in the Zhaheba area, it can be inferred that the regional D₁ compressive deformation most likely developed during the late Carboniferous to Permian (>276 Ma), whereas the D₂ deformation occurred during the compressional event in Permian (276–255 Ma).

In the Kalaan area, the Devonian–Carboniferous lithological units experienced both D₁ and D₂ deformations (Figure 8e). We propose that the eastern part of the central domain, where the Carboniferous Nanmingshui Formation is exposed (Figure 6a), experienced both D₁ and D₂ events. However, in the west part, the Upper Devonian–Lower Carboniferous Yundukala formations only experienced D₁ deformation (Figure 6a). Traditionally, the deposition of Yundukala Formation was considered as Devonian in age, but recent U–Pb zircon datings suggested an early Carboniferous maximum deposition ages of ca. 322 Ma (Jiang et al., 2024). In addition, the strata of the Yundukala Formation are intruded by a ca. 330 Ma granite (Liu et al., 2019), implying that at least part of this formation was deposited earlier. The Carboniferous age of the Nanmingshui Formation is roughly constrained by numerous shallow-marine fossils (BGMRX, 1978) and a granitic intrusion of ca. 323 Ma in the southern part of the study area (Liu et al., 2019). New U–Pb dating on the conglomeratic sandstone reveals a peak maximum deposition age of 310 ± 7 Ma for this Formation (Jiang et al., 2024), suggesting that the span of deposition of this formation ranges from ca. 323 to 310 Ma. Our new U–Pb zircon dating of sandstone adjacent to the northern part of the Nanmingshui Formation yields a maximum deposition age 263 ± 10 Ma, indicating its mid-Permian deposition (Figure 6). The deposition of these sedimentary rocks can be interpreted as an infill of minor, previously unmapped, post-orogenic or intra-montaneous syn-orogenic basins related to the Permian orogenic event.

The F₁ folding of the Yundukala and Nanmingshui strata started after their deposition, which should be sometime younger than ca. 310 Ma (Jiang et al., 2024). Based on the structural analysis, the granite (Sample 21FY14-2) intruded previously F₁ folded rocks but was truncated by the D₂ fault zone, implying that it was emplaced after D₁ but before the regional D₂ deformation (Figure 6a). Therefore, the available zircon age of 282 ± 5 Ma obtained from this granite indicates minimum age of D₁ and maximum age of D₂ deformations. Moreover, the age of the D₂ deformation can be constrained by the 269 ± 9 Ma undeformed granite–pegmatite dykes (Sample 21FY47-2) that were emplaced parallel to the axial plane of the F₂ folds (Figure 9e). This age is close to mid-Permian (ca. 263 Ma) maximum depositional age of sandstone (Sample 21FY61-2), indicating the supply of the proximal source region with the presence of Permian granitoids. The sandstone can be considered to have been deposited in a syn-orogenic basin, which is consistent with the presence of ca. 255 Ma syn-tectonic dykes, both suggesting a prolonged D₂ deformation (Figure 12b). Based on the available age data, it can be inferred that the D₁ deformation most likely developed during the late Carboniferous to early Permian (310–282 Ma), while the D₂ deformation occurred during the middle Permian (282–255 Ma), with a possible peak around ca. 269–263 Ma.

In summary, the combining structural geology and geochronology provide valuable insights into the timing of regional D₁ and D₂ deformations of the Zhaheba and Kalaan areas. The data from both regions indicate that the D₁ event occurred during ca. 310 and 282 Ma, while the D₂ event occurred within a time span of ca. 269 Ma (this study) and 255 Ma (Chen et al., 2013). However, it is likely that the D₂ could continue till Triassic times as suggested by Lehmann et al. (2010) or Schulmann et al. (2023).

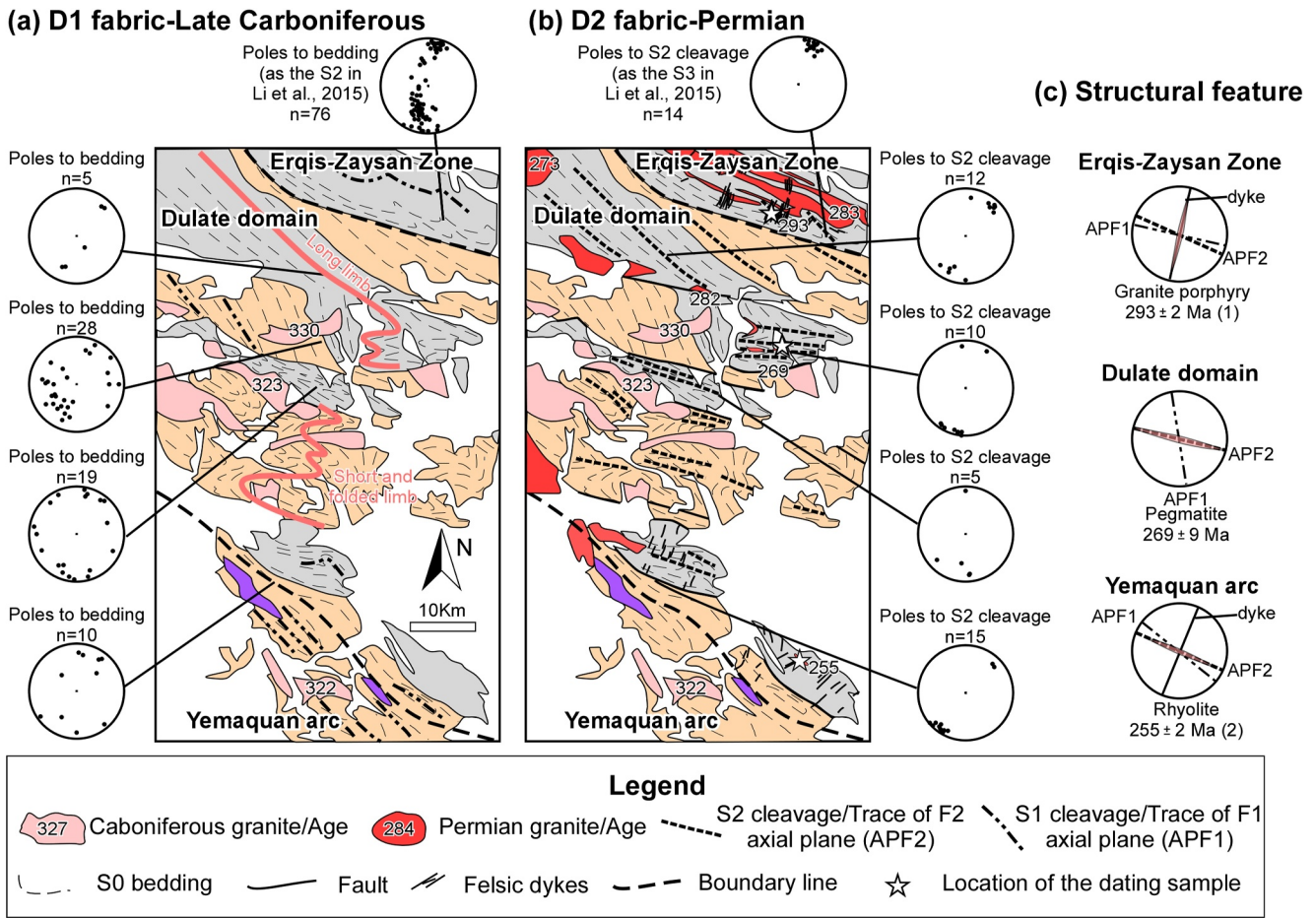


Figure 12. (a) The regional distribution of S_0 bedding and the D_1 fabrics in the East Junggar. (b) D_2 structural fabrics. (c) Restoration of D_1 fold axial planes of fabrics, and D_2 fold axial planes of the East Junggar.

7.2. Regional Patterns of D_1 and D_2 Deformations

In the East Junggar, two types of D_1 structural patterns can be identified (Figure 12). The first type is characterized by coherent packages of NW-trending steeply dipping beddings in the northern parts of the Yemaquan arc and Dulate domain. The S_0 dips steeply either to the NE or to the SW, indicating the existence of upright F_1 folds (Figure 12a). In the northern parts of the Yemaquan arc, the S_0 is entirely transposed by the $N330^\circ$ -trending axial planar cleavage S_1 . The second type of D_1 structural pattern is preserved in the central and southern parts of the Dulate domain (Figure 12a), where the D_1 fabric is affected by F_2 folds and partially transposed by S_2 cleavage. After unfolding the pattern of F_2 folds, the original sub-vertical bedding restores to a N–S trending direction (Figure 12c).

The D_2 deformation can also be divided into two principal types, as shown in Figure 12b. The northern Yemaquan arc exhibits dextral shearing, manifested by asymmetric folding of S_1 fabrics. This dextral shear zone separates the metamorphic rocks of the northern part of the Yemaquan arc from the Dulate domain to the NE. The Dulate domain itself is heterogeneously reworked by D_2 , with the highest intensity in the center and the south, where axial planar $N280$ – 290° trending S_2 cleavage develops. The characteristic feature is the presence of similar WNW–ESE trending ca. 255 Ma alkali-rich dykes that are parallel to the axial plane of the F_2 folds (Figure 12b). In the north, pegmatite dykes dated at 269 Ma (this work) can be considered as axial plane type fractures further confirming the direction of D_2 compression (Figure 12b). Importantly, NNE–SSW trending dykes are well known in the EZZ, where they crosscut the F_2 upright folds and their emplacement age was estimated to be 290–280 Ma (Shu et al., 2022). Moreover, the S_1 – S_2 fabric in the central and northern Dulate domain is roughly sub-parallel to the axial planes of F_2 upright folds affecting high grade metamorphic fabric of the EZZ (Li, Sun, et al., 2015). In

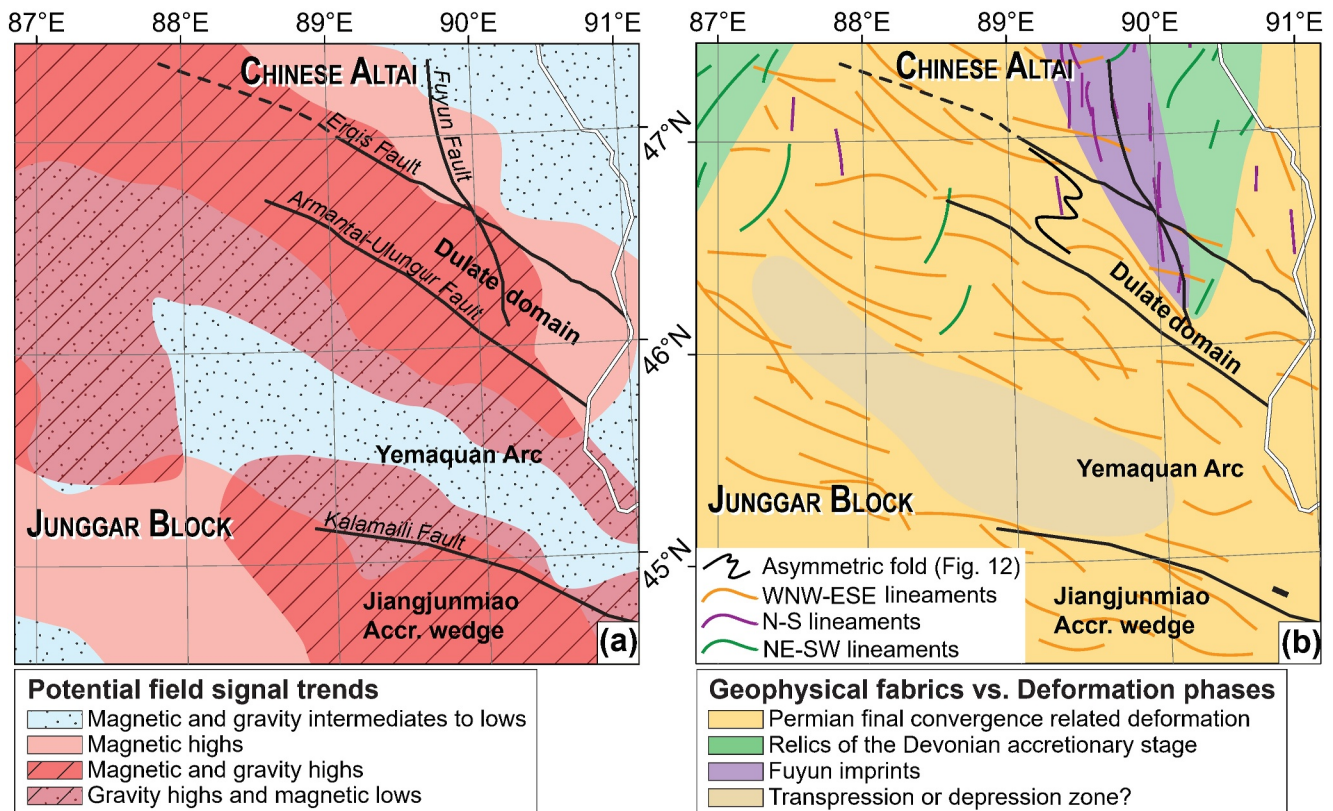


Figure 13. Correlation of potential field trends with the tectonic and deformation zones.

summary, like the southern part of the Chinese Altai, the EZZ reveals similar structural geometries of emplacement of dykes and synchronous upright folding with those in the southern Dulate domain (Li, Yuan, et al., 2015; Shu et al., 2022). However, it is important to note that this late deformation occurred 10–20 Ma earlier in the north compared to the south.

It can be concluded that prior to the D_2 deformation, the orogenic fabrics in the majority area of the East Junggar were originally trending in the NNW–SSE direction (Figure 12c). Following the D_2 deformation, these fabrics formed the large-scale asymmetrical folds, of which the long limbs rotated to the NW–SE direction in the northern Dulate domain and Yemaquan arc (Figure 12b). Meanwhile, the central Dulate domain represents a short and folded limb of this crustal-scale F_2 fold (Figure 12a). The D_2 deformation is associated with the significant NNE–SSW shortening of the entire East Junggar and the development of a generalized NNW–SSE trend across the whole Permian orogenic system, which is parallel with the boundary of East Junggar and Chinese Altai (Figure 12b).

7.3. Tectonic Interpretation of Geophysical Data

The analysis of magnetic and gravity signals provides insights on the basement structures, deep tectonic features, and imbrication of the different tectonic units in the junction area between the Chinese Altai in the north and the East Junggar and Junggar Block in the west (Figure 13). The Dulate domain and the Jiangjunmiao accretionary wedge mostly coincide with magnetic and gravity highs. Gravity highs straddle the Erqis, Armantai-Ulungur, and Kalamaili fault zones (Figure 13a). The gravity and magnetic highs straddling the Erqis fault zone were modeled as the underthrusting of the East Junggar beneath the Chinese Altai (Guy et al., 2021; Figure 14). Similarly, the gravity high straddling the Armantai-Ulungur may be interpreted as a stacking of volcano-sedimentary material due to the underthrusting of the Yemaquan arc beneath the Dulate domain, which is coherent with the dominant polarity of geophysical anomalies (Figures 11e and 11f). The center of the Yemaquan arc presents magnetic and gravity signatures varying from intermediate to low. In contrast, its southern and northern boundaries mostly correspond to gravity highs with magnetic lows in some parts (Figure 13a). In addition, one prominent, sub-

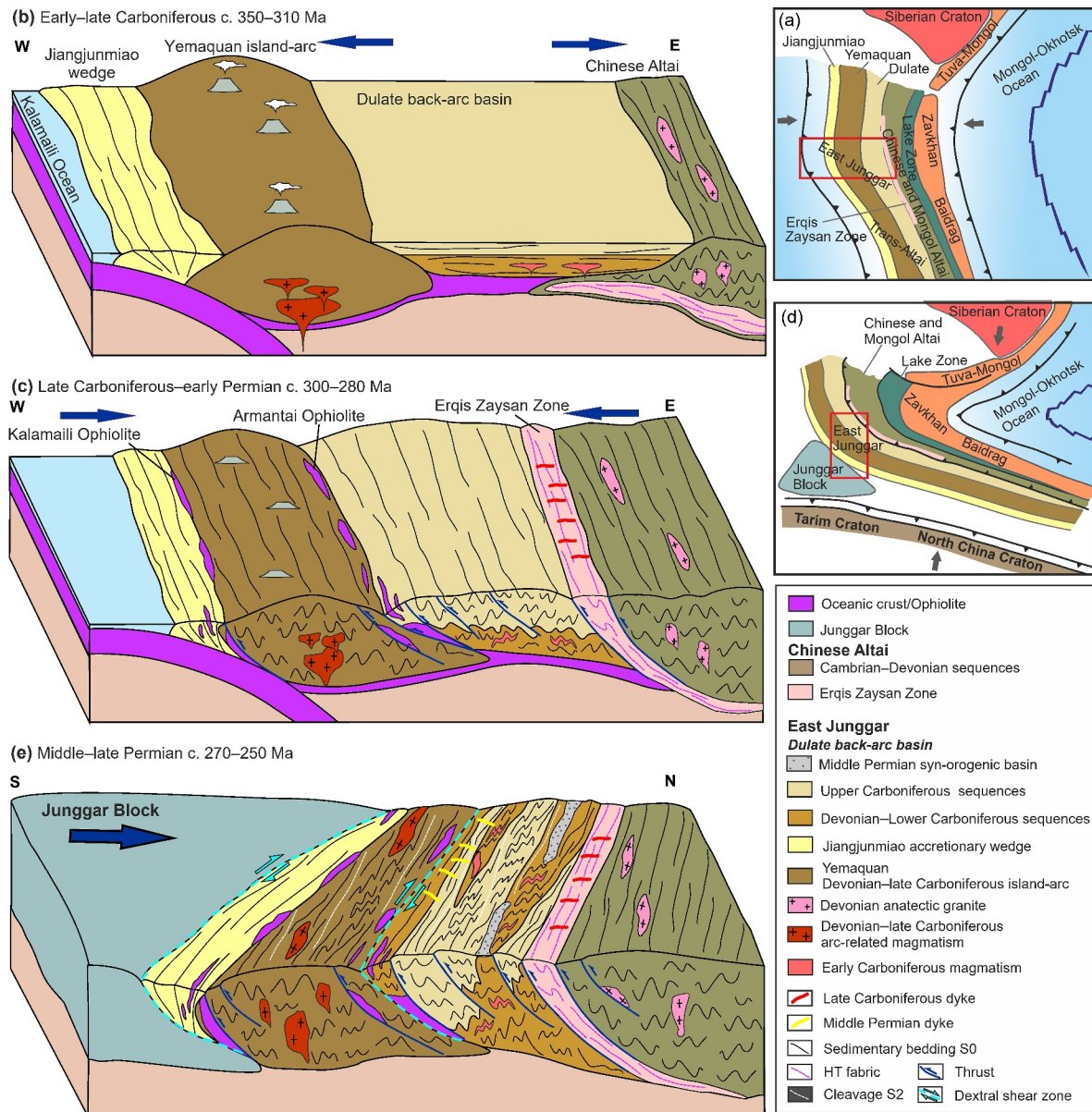


Figure 14. (a–c) Tectonic switch from retreating to advancing mode of the Kalamaili subduction system. (d) Scissor-like closure of the Mongol-Okhotsk Ocean to the north, anticlockwise rotation of southern limb of Mongolian orocline. (e) The Junggar block represents a rigid wedge-shaped promontory that deformed progressively shortened East Junggar subduction system.

vertical, and deep-seated magnetic contrast is located in the center of the Yemaquan arc, which can also be identified in the gravity anomalies by fragmented shallow sourced sub-vertical contrasts (Figures 11e and 11f). This sub-vertical boundary does not correspond to any documented surface lithological contrast and may be interpreted as the underthrusting of the Junggar Block beneath the East Junggar domain. The Erqis, Armantai-Ulungur, and Kalamaili faults cannot be delimited by such significant magnetic and gravity gradients, indicating that there are probably shallow faults and cannot be considered sites of important sutures, as suggested by previous works (Niu et al., 2007; Xiao et al., 2009).

The extraction of magnetic and gravity lineaments highlights and quantifies the importance of the deformation events. Three groups of lineaments can be distinguished in the East Junggar (Figure 13b). The extensive WNW–ESE-oriented geophysical fabrics are sub-parallel to the zones, where ophiolitic mélanges such as the Armantai and the Kalamaili ophiolites have been exhumed. These fabrics are distributed across the Chinese Altai, the East

Junggar and the Junggar Block. Structural analyses reveal that these WNW–ESE-oriented geophysical fabrics are sub-parallel to prominent D_2 cleavage zones and F_2 folds (Figure 12b), similar to those high-strain zones in the adjacent continuation from the East Junggar to the Trans-Altai Zone (Guy et al., 2021; Guy, Schulmann, Clauer, et al., 2014). Therefore, it is likely that these geophysical fabrics formed as the result of the Permian shortening in the whole East Junggar (Figure 13b). The deep-seated contacts associated with these fabrics dip mainly to the NE and less to the SW (Figures 11e and 11f). This demonstrates the general vergence of the Permian–Triassic tectonic event, probably linked to the development of NE-dipping thrust imbricates on a regional scale, as also supported by field observations at the boundary between the Chinese Altai and East Junggar (e.g., Briggs et al., 2007; Guy et al., 2020; Jiang et al., 2019). Deeply rooted anomalies indicate a rather thick-skinned thrusting mode at the scale of the whole East Junggar.

A NW–SE-oriented “corridor” without any magnetic and gravity lineament is observed in the central part of the Yemaquan arc, which is correlated with a magnetic low and an intermediate gravity signal (Figure 13b). In the West Junggar, a similar area marked by absence of lineaments, corresponds to a transpression zone dominated by simple shear at the boundary between the Junggar Block and the West Junggar (Miao, Zhang, Schulmann, Guy, et al., 2023). Alternatively, this can be interpreted as evidence of a basement depression of the Junggar Block due to its underthrusting beneath the West and East Junggar (Figure 14). The NE–SW-oriented lineaments are scattered in the Chinese Altai and to a lesser extent in the north-east of East Junggar (Figure 13b). These lineaments were interpreted as the remnants of the Devonian–Carboniferous compressional phase (Guy et al., 2020). The N–S-oriented lineaments, densely packed around the Fuyun fault, are interpreted as the imprints of Cenozoic dextral strike-slip deformation (Briggs et al., 2009). On the other hand, according to the satellite structural data presented in this study and their summary, the N–S-oriented lineaments in the northern Dulute domain are roughly parallel to the trend of axial planes of F_1 folds (Figures 8a and 12). Therefore, these lineaments in the northern Dulute domain possibly originated during the D_1 shortening deformation. It is likely that some lineaments with a WNW–ESE orientation in the D_2 deformation zones can be attributed to the reorientation of deep-seated D_1 fabrics, such as zones of the exhumation of the oceanic crust and the mantle (Figure 13b), exemplified by the Armantai ophiolite. Finally, the paucity of D_1 lineaments can be explained by their superficial thin-skinned nature in the Dulute domain.

7.4. Geodynamic Constraints on the East Junggar Supra-Subduction System

Most authors consider the Chinese Altai as an early Paleozoic accretionary wedge prior to extensive reworking by Devonian metamorphism and magmatism (Huang et al., 2020; Jiang et al., 2016). In contrast, the southern East Junggar mainly consists of unmetamorphosed volcanic-sedimentary complexes that have been interpreted as a system of accreted Devonian–Carboniferous island arcs (Wang et al., 2009, 2023; Windley et al., 2002, 2007; Xiao et al., 2004) reported the distinct Nd–Hf isotopic signatures, indicating that the East Junggar crust is significantly more juvenile compared to the Chinese Altai. These differences between the two crustal domains have led many scholars to conclude that they should represent two contrasting terranes that were juxtaposed during Permian sinistral translation along the continental-scale Erqis fault (Buslov et al., 2004; Laurent-Charvet et al., 2003; Windley et al., 2007).

However, new structural, detrital zircon and geophysical investigations along this critical Chinese Altai and East Junggar boundary provides a different picture. A detrital zircon study by Long, Yuan, Sun, Xiao, et al. (2012), Long, Yuan, Sun, Safonova, et al. (2012) revealed that the Cambrian and Ordovician age peaks in the Devonian and Carboniferous strata of East Junggar are identical to those in the Chinese Altai, indicating that the two regions belonged to the same oceanic domain during the Paleozoic era. Structural investigations show SW-directed imbricated thrusts and NW–SE-trending upright folds affecting the EZZ and the Chinese Altai, indicating compressional regime orthogonal to this boundary (Briggs et al., 2007; Broussolle et al., 2018; Jiang et al., 2019). Furthermore, new geophysical studies suggest that the East Junggar deep crust was underthrust at least 50 km beneath the Chinese Altai and that the trace of the Erqis fault does not coincide with major geophysical lineaments (Guy et al., 2020, 2021). These observations invalidate concept of large-scale sinistral translation along the deep-seated Erqis fault and indicate that the frontal convergence between the two domains is more likely.

Recently Jiang et al. (2024) proposed a different model in which the Dulute domain formed as a Carboniferous back-arc basin related to the north dipping Kalamaili oceanic subduction. According to this model, the Yemaquan arc was formed in the north of this subduction system (current coordinates) and provided detritus to the northern

back arc basin. This basin also received material from the northerly Chinese Altai (Figures 14a and 14b). Therefore, the Dulute domain and Yemaquan arc most likely represented island arc/marginal sea that separated the Cambrian–Ordovician East Junggar oceanic crust, which is exposed in areas like Zhaheba area from the Chinese Altai wedge to the north. Jiang et al. (2024) also proposed that the opening of the Dulute back-arc system was related to the rollback of the Kalamaili subduction zone and involved a significant stretching and melting of fertile sedimentary rocks at ca. 320–310 Ma.

Therefore, the age of deformation fabrics, finite strain pattern and geophysical data of both Yemaquan arc and Dulute domain, presented in this study, play an essential role in understanding the geodynamic evolution of this complex region. The D_1 deformation occurred after the deposition of back-arc sequences and is likely associated with the closure of the back-arc system and an end of activity of the Yemaquan arc. The ca. 315 Ma fore-arc sedimentary rocks unconformably covering the Jiangjunmiao accretionary complex suggests that the Yemaquan arc was still active during the Late Carboniferous (Huang et al., 2018). On the other hand, the subduction of the Dulute back-arc crust beneath the Chinese Altai is constrained by the ca. 313 Ma arc-related magmatism in the Chinese Altai (Cai et al., 2012).

Our structural and geophysical study shows that the Armantai mélangé in the Zhaheba area represents a surface expression of imbricated thrust, along which the fragments of the Cambrian–Ordovician oceanic crust and mantle are exhumed (Figures 14a–14c). Importantly, the northern Yemaquan arc and southern Dulute domain reveal a structural continuity in terms of the D_1 folding style, fabric parallelism and age of deformation (Figure 12). As mentioned earlier, the Armantai mélangé in the Zhaheba area is also located on the northern slope of a major NW–SE-trending magnetic and gravity high (Figure 13). This anomaly is associated with opposite polarities (Figure 11), further supporting the possible existence of a deep-seated cusped structure or a blind fault. On the other hand, the magnetic anomaly is connected to the NE-oriented polarities, which corresponds to a general thick-skinned imbrications of the East Junggar basement (Guy et al., 2020). The Dulute back-arc system in the Zhaheba and Kalaan areas was also affected by the D_1 folding that occurred after 310 Ma but before 282 Ma (Figure 12). This time frame aligns with the ages of late Carboniferous to early Permian high-pressure granulite-facies metamorphism developed in the southern edge of the EZZ (Li et al., 2022). The high-pressure event was followed by the NNE–SSW compression that is characterized by upright folding and intrusion of vertical NNE–SSW-trending granite dykes dated at ca. 300–280 Ma (e.g., Li et al., 2017; Shu et al., 2022). All these data, combined with the gravity and magnetic anomalies and the lineaments with predominantly NE-dipping geophysical contrasts, indicate the general underthrusting of the East Junggar beneath the Chinese Altai (e.g., Briggs et al., 2007; Guy et al., 2020, 2021; Jiang et al., 2019). Taken together, the ages of Dulute back-arc volcanic-sedimentary sequences presented by Jiang et al. (2024) and the D_1 shortening of the whole Yemaquan–Dulute supra-subduction system point to a subduction switch from the late Carboniferous extension to the early Permian compression (Figures 14a and 14b). This tectonic switch can be explained by the evolution from a retreating to advancing mode of the Kalamaili subduction system in the same coordinates (Figures 14a–14c).

The structural data presented in this study, as well as those published from the Chinese Altai, indicate that the orogenic fabrics of both the East Junggar and the Chinese Altai were oriented roughly in the NNE–SSW direction during the late Carboniferous (e.g., Guy et al., 2020; Kong et al., 2022; Xu et al., 2021). Although the orientation of compressive structures in the Chinese Altai was acquired in late Devonian (e.g., Kong et al., 2022), the data of this study and those from equivalent units in Mongolia (Lehmann et al., 2010) indicate a continuous E–W-directed (current coordinates) shortening during the late Carboniferous (ca. 310–300 Ma). Altogether, the data presented in this work confirm that the coordinate framework of shortening-extensional cycles remained the same for the whole Paleozoic era for both the Chinese Altai and the East Junggar.

7.5. Middle to Late Permian Collisional Deformation of the East Junggar

The D_2 deformation is primarily associated with the NNE–SSW shortening of all previous structures and the tectonic discontinuities of the East Junggar domain. The deformation, which occurred in the Permian at ca. 270–250 Ma (Guadalupian to Lopingian), also affected the Chinese Altai and reworked precisely dated pegmatite dyke swarms (Jiang et al., 2019; Miao, Zhang, Schulmann, Lexa, et al., 2023; Shu et al., 2022). The D_2 deformation led to the reorientation of the late Devonian to early Carboniferous upright folds into a WNW–ESE direction along the whole southern margin of the Chinese Altai (Kong et al., 2022; Miao, Zhang, Schulmann, Lexa, et al., 2023; Xu et al., 2021). This deformation is also related to the extrusion of granulite-facies rocks and migmatites in core

of large antiforms (Broussolle et al., 2018). The geophysical data further show that this area corresponds to the tip of East Junggar promontory buried deeply beneath the Chinese Altai (Guy et al., 2020). The deep crust was further underthrust beneath the Chinese Altai (e.g., Shu et al., 2022). All of these deformations should have occurred after the Permian anticlockwise rotation of the southern limb of the Mongolian Orocline (Edel et al., 2014; Schulmann et al., 2023).

During the D_2 deformation, the upper crust of the East Junggar domain experienced upright folding at a high angle to D_1 fabrics. Our study reveals that in the Zhaheba region, the D_1 fabrics were reworked by the dextral NW–SE-trending transpressive shear zone during the D_2 deformation. This structural pattern can be interpreted as a result of dextral shearing parallel to the Junggar basement promontory (Figures 14d and 14e). The zone of dextral shearing is narrower in the east than in the west, possibly indicating a higher convergence angle of the basement boundary (Ježek et al., 2002). However, the pure shear dominated shortening affected the rest of the East Junggar, indicating that the indentation of Junggar Block and shortening of the whole East Junggar edifice were coevally coupled. The D_2 shortening resulted in the formation of crustal scale asymmetrical folds, where the long limbs are reoriented parallel to the Chinese Altai–East Junggar boundary and the main Armantai and Kalamaili faults, whereas the short limbs retain more or less the orientation of D_1 fabrics in the central parts of the Dulate domain and Yemaquan arc (Figures 12b and 14e). However, the origin of D_1 and D_2 orthogonal superposition was also explained previously by a model of axial plane cleavage fanning and folding during progressive deformation (e.g., Edel et al., 2014). In that model, the Late Carboniferous early axial planar cleavage rotated together with the southern limb of the Mongolian orocline, so that the local stress field became orthogonal after this critical rotation (Van der Voo, 2004; Viola & Mancktelow, 2005; Treagus, 1973). In contrast, if it is taken into account that the geometry of the Yemaquan arc and the Dulate back-arc extension together with their shortening was in the same coordinate (Figure 14c), the model of tectonic switching followed by the Permian orthogonal shortening should be preferable.

This shortening, reported from easterly Trans-Altai Zone (Lehmann et al., 2010), was attributed to the scissor-like closure of the Mongol Okhotsk Ocean to the north, the anticlockwise rotation of southern limb of Mongolian Orocline (Figure 14d), and the collision of the Tarim–North China cratons collage with the Mongolian collage. The Junggar Block represents a rigid wedge-shaped promontory that progressively shortened the East Junggar subduction system located between the Tarim–North China collage in the south and the Mongolian Orocline in the north (Figure 14d).

Altogether, the present study shows the importance of regional structural, satellite imagery and geophysical studies accompanied by modern geochronological constraints of superposed deformation events for large scale tectonic models. Similar previous studies carried in the Chinese Altai (Guy et al., 2020), southern Mongolia in the east (Guy, Schulmann, Clauer, et al., 2014; Guy, Schulmann, Munsch, et al., 2014) and Beishan in the SE (Tian et al., 2013). The latter analyses confirmed that the switch in shortening directions occurred in Permian time and the final N–S shortening continued till the early Jurassic (Schulmann et al., 2023). The extension of such studies to the Kazakhstan orocline in the west and reevaluation of tectonic switch in the Trans-Altai zone to the east (Guy, Schulmann, Clauer, et al., 2014; Lehmann et al., 2010), Tarim–North China collage to the south (e.g., Li, He, et al., 2020) and Mongol–Okhotsk domain to the north (e.g., Liang et al., 2018) will bring decisive constraints into our understanding of formation of both Kazakstan and Mongolia oroclinal systems in future.

8. Conclusions

1. The northern Yemaquan arc domain shows pervasive development of WNW–ESE D_1 cleavage and tight upright F_1 folds, which are related to the exhumation of Armantai ophiolitic mélangé in a dome-like structure. The Dulate back-arc domain shows development of N–S trending upright F_1 folds that are preserved in the low-strain domains. The age of D_1 deformation is constrained by ca. 310 Ma back-arc sedimentary rocks and the ca. 282 Ma post- D_1 granitic intrusion.
2. In the Dulate domain, the NNW–SSE trending F_1 folds are reworked by nearly orthogonal Permian D_2 shortening, resulting in the formation of Ramsay's Type 1 dome-and-basin interference pattern and the zones of widespread E–W trending S_2 cleavage. Meanwhile, a dextral transpressive shear zone separated the Yemaquan arc from the Dulate back-arc system parallel the eastern margin of Junggar block. The age of D_2 is constrained by the ca. 269 Ma syntectonic pegmatites and the deposition of ca. 263 Ma syn-orogenic sedimentary rocks.

3. The late Carboniferous D₁ structures in the East Junggar formed due to closure of the Dulate back-arc basin, which was caused by the eastward advance of the Kalamaili subduction system. The nearly orthogonal Permian D₂ fabrics resulted from the massive N–S shortening of the East Junggar and the northward movement of the Junggar Block indenter.
4. The D₂ deformation was related to the anticlockwise rotation of the southern limb of the Mongolian Orocline, the scissor-like closure of the northerly Mongol-Okhotsk Ocean and the collision of the Mongolian and the Tarim-North China craton collages.

Data Availability Statement

The zircon U–Pb data used for constraining the timing of the regional D1 and D2 deformations in the study are available in the Supporting Information_Tables. The gravity and magnetic data used in this study come respectively from the EGM08 (Pavlis et al., 2012; Data set is available at <http://earth-info.nga.mil/GandG/wgs84/gravitymod/egm2008/>) and EMAG2 (Maus et al., 2009; Data set is available at <https://www.ngdc.noaa.gov/geomag/emag2.html>) models.

Acknowledgments

We thank journal editor Prof. Djordje Grujic, associate editor, reviewers Prof. Peter Cawood and Prof. Gaoxue Yang for their insightful comments, which helped us significantly improve the manuscript. This study was financially supported by the National Outstanding Youth Science Fund Project of National Natural Science Foundation of China (42025204); National Key Research and Development Program of China (No. 2023YFF0803804); Grant Agency of the Czech Republic (GAČR EXPRO Grant GX19-27682X); International Partnership Program of Chinese Academy of Sciences (132744KYSB20190039).

References

- An, R., Zhao, G., Liu, Q., & Han, Y. (2021). Early Palaeozoic subduction-accretion in East Junggar (NW China): Insights from age, geochemical, and Sr–Nd–Hf isotopic data of andesitic rocks in the northern Yemaquan Arc. *Lithos*, 380–381, 380–381. <https://doi.org/10.1016/j.lithos.2020.105892>
- Archibald, N., Gow, P., & Boschetti, F. (1999). Multiscale edge analysis of potential field data. *Exploration Geophysics*, 30(1–2), 38–44. <https://doi.org/10.1071/eg999038>
- Briggs, S. M., Yin, A., Manning, C. E., Chen, Z.-L., & Wang, X.-F. (2009). Tectonic development of the southern Chinese Altai Range as determined by structural geology, thermobarometry, 40Ar/39Ar thermochronology, and Th/Pb ion-microprobe monazite geochronology. *Geological Society of America Bulletin*, 121(9–10), 1381–1393. <https://doi.org/10.1130/b26385.1>
- Briggs, S. M., Yin, A., Manning, C. E., Chen, Z. L., Wang, X. F., & Grove, M. (2007). Late Paleozoic tectonic history of the Ertix Fault in the Chinese Altai and its implications for the development of the Central Asian Orogenic System. *Geological Society of America Bulletin*, 119(7–8), 944–960. <https://doi.org/10.1130/b26044.1>
- Broussole, A., Aguilar, C., Sun, M., Schulmann, K., Štípská, P., Jiang, Y., et al. (2018). Polycyclic Palaeozoic evolution of accretionary orogenic wedge in the southern Chinese Altai: Evidence from structural relationships and U–Pb geochronology. *Lithos*, 314–315, 400–424. <https://doi.org/10.1016/j.lithos.2018.06.005>
- Bureau of Geology and Mineral Resources of Xinjiang Autonomous Region (BGMRX). (1978). Geological map and explanatory note of the Fuyun sheet: BGMRX, scale 1:200,000.
- Burkhard, M. (1990). Calcite twins, their geometry, appearance and significance as stress-strain markers and indicators of the tectonic regime: A review. *Journal of Structural Geology*, 15(3–5), 351–368. [https://doi.org/10.1016/0191-8141\(93\)90132-t](https://doi.org/10.1016/0191-8141(93)90132-t)
- Buslov, M. M., Watanabe, T., Fujiwara, Y., Iwata, K., Smirnova, L. V., Safonova, I. Y., et al. (2004). Late Paleozoic faults of the Altai region, central Asia: Tectonic pattern and model of formation. *Journal of Asian Earth Sciences*, 23(5), 655–671. [https://doi.org/10.1016/s1367-9120\(03\)00131-7](https://doi.org/10.1016/s1367-9120(03)00131-7)
- Cai, K., Sun, M., Yuan, C., Xiao, W., Zhao, G., Long, X., & Wu, F. (2012). Carboniferous mantle-derived felsic intrusion in the Chinese Altai, NW China: Implications for geodynamic change of the accretionary orogenic belt. *Gondwana Research*, 22(2), 681–698. <https://doi.org/10.1016/j.gr.2011.11.008>
- Cai, X., Fan, G., Wang, F., Liao, Q., & Tian, J. (2018). New progress on the study of Devonian Kalamaili Formation in East Junggar, Xinjiang. *Bulletin of Mineralogy, Petrology and Geochemistry*, 34, 849–860. (in Chinese with English abstract).
- Chen, Y., Wang, Y., Wang, J., Ding, R., Yuan, Y., & Shi, Y. (2013). Zircon U–Pb age, geochemistry and geological implication of the 255 Ma Alkali-rich dykes from Ulungur area, North Xinjiang. *Journal of Earth Sciences*, 24(4), 519–528. <https://doi.org/10.1007/s12583-013-0346-x>
- Choulet, F., Cluzel, D., Faure, M., Lin, W., Wang, B., Chen, Y., et al. (2012). New constraints on the pre-Permian continental crust growth of Central Asia (West Junggar, China) by U–Pb and Hf isotopic data from detrital zircon. *Terra Nova*, 24(3), 189–198. <https://doi.org/10.1111/j.1365-3121.2011.01052.x>
- Choulet, F., Faure, M., Cluzel, D., Chen, Y., Lin, W., & Wang, B. (2012). From oblique accretion to transpression in the evolution of the Altaid collage: New insights from West Junggar, northwestern China. *Gondwana Research*, 21(2–3), 530–547. <https://doi.org/10.1016/j.gr.2011.07.015>
- Choulet, F., Faure, M., Cluzel, D., Chen, Y., Lin, W., Wang, B., & Xu, B. (2016). Toward a unified model of Altaids geodynamics: Insight from the Palaeozoic polycyclic evolution of West Junggar (NW China). *Science China Earth Sciences*, 59(1), 25–57. <https://doi.org/10.1007/s11430-015-5158-7>
- Edel, J. B., Schulmann, K., Hanžl, P., & Lexa, O. (2014). Palaeomagnetic and structural constraints on 90° anticlockwise rotation in SW Mongolia during the Permo–Triassic: Implications for Altaid oroclinal bending. Preliminary palaeomagnetic results. *Journal of Asian Earth Sciences*, 94, 157–171. <https://doi.org/10.1016/j.jseas.2014.07.039>
- Geng, H., Sun, M., Yuan, C., Zhao, G., & Xiao, W. (2011). Geochemical and geochronological study of early Carboniferous volcanic rocks from the West Junggar: Petrogenesis and tectonic implications. *Journal of Asian Earth Sciences*, 42(5), 854–866. <https://doi.org/10.1016/j.jseas.2011.01.006>
- Guy, A., Schulmann, K., Clauer, N., Hasalová, P., Seltmann, R., Armstrong, R., et al. (2014). Late Paleozoic–Mesozoic tectonic evolution of the Trans-Altai and South Gobi Zones in southern Mongolia based on structural and geochronological data. *Gondwana Research*, 25(1), 309–337. <https://doi.org/10.1016/j.gr.2013.03.014>
- Guy, A., Schulmann, K., Munschy, M., Mieke, J. M., Edel, J. B., Lexa, O., & Fairhead, D. (2014). Geophysical constraints for terrane boundaries in southern Mongolia. *Journal of Geophysical Research: Solid Earth*, 119(10), 7966–7991. <https://doi.org/10.1002/2014jb011026>

- Guy, A., Schulmann, K., Soejono, I., Holzrichter, N., Lexa, O., & Munsch, M. (2021). Structures and geodynamics of the Mongolian tract of the Central Asian Orogenic Belt constrained by potential field analyses. *Gondwana Research*, 92, 26–53. <https://doi.org/10.1016/j.gr.2020.11.016>
- Guy, A., Schulmann, K., Soejono, I., & Xiao, W. (2020). Revision of the Chinese Altai-East Junggar terrane accretion model based on geophysical and geological constraints. *Tectonics*, 39(4). <https://doi.org/10.1029/2019tc006026>
- Holden, D. J., Archibald, N. J., Boschetti, F., & Hessel, M. W. (2000). Inferring geological structures using wavelet-based multiscale edge analysis and forward models. *Exploration Geophysics*, 31(4), 67–71. <https://doi.org/10.1071/EG00617>
- Hong, T., Klemd, R., Gao, J., Xiang, P., Xu, X.-W., You, J., et al. (2017). The tectonic evolution of the Irtysh tectonic belt: New zircon U–Pb ages of arc-related and collisional granitoids in the Kalaxiangar tectonic belt, NW China. *Lithos*, 272–273, 46–68. <https://doi.org/10.1016/j.lithos.2016.12.001>
- Hornby, P., Boschetti, F., & Horowitz, F. G. (1999). Analysis of potential field data in the wavelet domain. *Geophysical Journal International*, 137(1), 175–196. <https://doi.org/10.1046/j.1365-246x.1999.00788.x>
- Huang, B., Fu, D., Kusky, T., Ruan, K., Zhou, W., & Zhang, X. (2018). Sedimentary provenance in response to Carboniferous arc-basin evolution of East Junggar and North Tianshan belts in the southwestern central Asian orogenic belt. *Tectonophysics*, 722, 324–341. <https://doi.org/10.1016/j.tecto.2017.11.015>
- Huang, H., Niu, G., Wang, X., Guo, J., & Yu, F. (2012). Formation and emplacement age of Karamaili ophiolite: LA-ICP-MS zircon U–Pb age evidence from the diabase and tuff in eastern Junggar, Xinjiang. *Geological Bulletin of China*, 31(8), 12.
- Huang, Y., Jiang, Y., Collett, S., Wang, S., Xu, K., Shu, T., et al. (2020). Magmatic recycling of accretionary wedge: A new perspective on Silurian–Devonian I-type granitoids generation in the Chinese Altai. *Gondwana Research*, 78, 291–307. <https://doi.org/10.1016/j.gr.2019.07.019>
- Ježek, J., Schulmann, K., & Thompson, a. B. (2002). Strain partitioning in front of an obliquely convergent indenter. *EGU Stephan Mueller Special Publ Ser.*, 1, 93–104. <https://doi.org/10.5194/smsps-1-93-2002>
- Jiang, Y., Tan, S., Soejono, I., Nádaskay, R., Schulmann, K., Ning, J., et al. (2024). Late Paleozoic sedimentation recording back-arc basin evolution in response to the Chinese Altai-East Junggar convergence in Central Asia. *Geological Society of America Bulletin*. <https://doi.org/10.1130/B37247.1>
- Jiang, Y. D., Schulmann, K., Sun, M., Štípská, P., Guy, A., Janoušek, V., et al. (2016). Anatectis of accretionary wedge, Pacific-type magmatism, and formation of vertically stratified continental crust in the Altai Orogenic Belt. *Tectonics*, 35(12), 3095–3118. <https://doi.org/10.1002/2016tc004271>
- Jiang, Y. D., Schulmann, K., Sun, M., Weinberg, R. F., Štípská, P., Li, P. F., et al. (2019). Structural and geochronological constraints on Devonian Suprasubduction tectonic switching and Permian collisional dynamics in the Chinese Altai, central Asia. *Tectonics*, 38(1), 253–280. <https://doi.org/10.1029/2018tc005231>
- Kong, L., Jiang, Y., Schulmann, K., Zhang, J., Weinberg, R. F., Sun, M., et al. (2022). Petrostructural and geochronological constraints on Devonian extension-shortening cycle in the Chinese Altai: Implications for retreating-advancing subduction. *Tectonics*, 41(9). <https://doi.org/10.1029/2021tc007195>
- Laurent-Charvet, S., Charvet, J., Monié, P., & Shu, L. (2003). Late Paleozoic strike-slip shear zones in eastern central Asia (NW China): New structural and geochronological data. *Tectonics*, 22(2). <https://doi.org/10.1029/2001tc901047>
- Lehmann, J., Schulmann, K., Lexa, O., Corsini, M., Kroner, A., Štípská, P., et al. (2010). Structural constraints on the evolution of the central Asian orogenic belt in SW Mongolia. *American Journal of Science*, 310(7), 575–628. <https://doi.org/10.2475/07.2010.02>
- Li, A., Xu, Y., Liao, W., Han, B.-F., & Wei, C. (2022). High-pressure granulite-facies metamorphism in the junction between the Siberian and Kazakhstan–Junggar continents and implications for the assembly of Pangea. *Gondwana Research*, 110, 13–30. <https://doi.org/10.1016/j.gr.2022.06.006>
- Li, D., He, D., Sun, M., & Zhang, L. (2020). The role of arc-arc collision in accretionary orogenesis: Insights from ~320 Ma tectono-sedimentary transition in the Karamaili area, NW China. *Tectonics*, 39(1). <https://doi.org/10.1029/2019tc005623>
- Li, D., He, D.-f., Santosh, M., & Tang, J.-y. (2014). Petrogenesis of late Paleozoic volcanics from the Zhaheba depression, East Junggar: Insights into collisional event in an accretionary orogen of central Asia. *Lithos*, 184–187, 167–193. <https://doi.org/10.1016/j.lithos.2013.10.003>
- Li, P., Sun, M., Rosenbaum, G., Cai, K., & Yu, Y. (2015). Structural evolution of the Irtysh shear zone (northwestern China) and implications for the amalgamation of arc systems in the central Asian orogenic belt. *Journal of Structural Geology*, 80, 142–156. <https://doi.org/10.1016/j.jsg.2015.08.008>
- Li, P., Sun, M., Rosenbaum, G., Cai, K., Yuan, C., Jourdan, F., et al. (2020). Tectonic evolution of the Chinese Tianshan Orogen from subduction to arc-continent collision: Insight from polyphase deformation along the Gangou section, Central Asia. *GSA Bulletin*, 132(11–12), 2529–2552. <https://doi.org/10.1130/b35353.1>
- Li, P., Sun, M., Rosenbaum, G., Jourdan, F., Li, S., & Cai, K. (2017). Late Paleozoic closure of the Ob-Zaisan Ocean along the Irtysh shear zone (NW China): Implications for arc amalgamation and oroclinal bending in the Central Asian Orogenic Belt. *Geological Society of America Bulletin*, 129(5–6), 547–569. <https://doi.org/10.1130/b31541.1>
- Li, P., Yuan, C., Sun, M., Long, X., & Cai, K. (2015). Thermochronological constraints on the late Paleozoic tectonic evolution of the southern Chinese Altai. *Journal of Asian Earth Sciences*, 113, 51–60. <https://doi.org/10.1016/j.jseaeas.2014.11.004>
- Li, Z., Nie, F., Tian, X., Shi, Y., Niu, H., & Wang, C. (2016). Redefinition of formation age of late Paleozoic strata in the Eastern Junggar tectonic zone and its implications for evolution of regional geological structure. *Acta Geologica Sinica*, 90, 569–588.
- Liang, C., Liu, Y., Zheng, C., Li, W., Neubauer, F., Zhang, Q., & Zhang, D. (2018). Deformation patterns and timing of the thrust-nappe structures in the Mohe Formation in Mohe basin, northeast China: Implication of the closure timing of Mongol–Okhotsk ocean. *Geological Journal*, 54(2), 746–769. <https://doi.org/10.1002/gj.3502>
- Liu, W., Liu, X.-J., & Liu, L.-J. (2013). Underplating generated A- and I-type granitoids of the East Junggar from the lower and the upper oceanic crust with mixing of mafic magma: Insights from integrated zircon U–Pb ages, petrography, geochemistry and Nd–Sr–Hf isotopes. *Lithos*, 179, 293–319. <https://doi.org/10.1016/j.lithos.2013.08.009>
- Liu, X., & Liu, W. (2014). Source characteristics and tectonic setting of the early and middle Devonian volcanic rocks in the North Junggar, northwest China: Insights from Nd–Sr isotopes and geochemistry. *Lithos*, 184–187, 27–41. <https://doi.org/10.1016/j.lithos.2013.10.015>
- Liu, X., Liu, W., & Si, C. (2019). Petrogenesis and source rocks of the high-K calc-alkaline and shoshonitic I-type granitoids in the northwestern part of East Junggar, NW China. *Lithos*, 326–327, 298–312. <https://doi.org/10.1016/j.lithos.2018.12.033>
- Liu, X., Xiao, W., Xu, J., Castillo, P. R., & Shi, Y. (2017). Geochemical signature and rock associations of ocean ridge-subduction: Evidence from the Karamaili Paleo-Asian ophiolite in east Junggar, NW China. *Gondwana Research*, 48, 34–49. <https://doi.org/10.1016/j.gr.2017.03.010>
- Liu, Y., Jian, P., Zhang, W., Shi, Y., Wang, Y., Zhang, L., & Liu, D. (2016). Zircon SHRIMP U–Pb dating and O isotope of the Beitashan ophiolitic mélange in the East Junggar, Xinjiang, and its geological significance. *Acta Petrologica Sinica*, 32.

- Long, X., Yuan, C., Sun, M., Safonova, I., Xiao, W., & Wang, Y. (2012). Geochemistry and U–Pb detrital zircon dating of Paleozoic graywackes in East Junggar, NW China: Insights into subduction–accretion processes in the southern central Asian orogenic belt. *Gondwana Research*, 21(2–3), 637–653. <https://doi.org/10.1016/j.gr.2011.05.015>
- Long, X., Yuan, C., Sun, M., Xiao, W., Wang, Y., Cai, K., & Jiang, Y. (2012). Geochemistry and Nd isotopic composition of the Early Paleozoic flysch sequence in the Chinese Altai, Central Asia: Evidence for a northward-derived mafic source and insight into Nd model ages in accretionary orogen. *Gondwana Research*, 22(2), 554–566. <https://doi.org/10.1016/j.gr.2011.04.009>
- Luo, J., Xiao, W., Wakabayashi, J., Han, C., Zhang, J. e., Wan, B., et al. (2017). The Zhaheba ophiolite complex in Eastern Junggar (NW China): Long lived supra-subduction zone ocean crust formation and its implications for the tectonic evolution in southern Altai. *Gondwana Research*, 43, 17–40. <https://doi.org/10.1016/j.gr.2015.04.004>
- Maus, S., Barckhausen, U., Berkenbosch, H., Bournas, N., Brozena, J., Childers, V., et al. (2009). EMAG2: A 2-arc min resolution Earth magnetic anomaly grid compiled from satellite, airborne, and marine magnetic measurements [Dataset]. *Geochemistry, Geophysics, Geosystems*, 10(8), 1–12. <https://doi.org/10.1029/2009gc002471>
- Miao, Y., Zhang, J., Schulmann, K., Guy, A., Jiang, Y., Sun, M., et al. (2023). Crustal-scale Disharmonic structural pattern of West Junggar: Unveiling a Permian indentation of Junggar block into northern Kazakhstan orocline. *Tectonics*, 42(5). <https://doi.org/10.1029/2022tc007689>
- Miao, Y., Zhang, J., Schulmann, K., Lexa, O., Jęřábek, P., Sun, M., et al. (2023). Polyphase deformation of staurolite-bearing metapelite in the Chinese Altai: Recording a Devonian–Permian tectonic regime switch in the southwestern central Asian orogenic belt. *Journal of Structural Geology*, 174, 104917. <https://doi.org/10.1016/j.jsg.2023.104917>
- Miller, H. G., & Singh, V. (1994). Potential field tilt—A new concept for location of potential field sources. *Journal of Applied Geophysics*, 32(2), 213–217. [https://doi.org/10.1016/0926-9851\(94\)90022-1](https://doi.org/10.1016/0926-9851(94)90022-1)
- Niu, H. C., Shan, Q., Zhang, H. X., & Yu, X. Y. (2007). 40Ar/39Ar geochronology of the ultrahigh pressure metamorphic quartz–magnetite in Zhaheba, Eastern Junggar, Xinjiang. *Acta Petrologica Sinica*, 23, 1627–1634.
- Passchier, C. W., & Trouw, R. A. J. (2005). *Micro-tectonics* (p. 177). Springer.
- Pavlis, N. K., Holmes, S. A., Kenyon, S. C., & Factor, J. K. (2012). The development and evaluation of the Earth Gravitational Model 2008 (EGM2008) [Dataset]. *Journal of Geophysical Research*, 117(B4), 1–38. <https://doi.org/10.1029/2011jb008916>
- Ramsay, J. G. (1962). Interference patterns produced by the superposition of folds of similar type. *The Journal of Geology*, 70(4), 466–481. <https://doi.org/10.1086/626837>
- Ramsay, J. G. (1967). *Folding and fracturing of rocks*. McGraw-Hill.
- Schulmann, K., Edel, J. B., Lexa, O., Xiao, W., Trebinova, D., Spikings, R., et al. (2023). Paleomagnetic, tectonic and geochronological constraints for Permian–Triassic oroclinal bending of the Mongolian collage. *National Science Review*, 10(2), nwac184. <https://doi.org/10.1093/nsr/nwac184>
- Şengör, A. M. C., Natal'in, B. A., & Burtman, V. S. (1993). Evolution of the Altai tectonic collage and Palaeozoic crustal growth in Eurasia. *Nature*, 364(6435), 299–307. <https://doi.org/10.1038/364299a0>
- Shu, T., Jiang, Y., Schulmann, K., Yu, Y., Yuan, C., Wang, S., et al. (2022). Structure, geochronology, and petrogenesis of Permian peraluminous granite dykes in the southern Chinese Altai as indicators of Altai–East Junggar convergence. *GSA Bulletin*. <https://doi.org/10.1130/b36408.1>
- Song, P., Wang, T., Tong, Y., Zhang, J., Huang, H., & Qin, Q. (2019). Contrasting deep crustal compositions between the Altai and East Junggar orogens, SW central Asian orogenic belt: Evidence from zircon Hf isotopic mapping. *Lithos*, 328–329, 297–311. <https://doi.org/10.1016/j.lithos.2018.12.039>
- Su, Y., Zheng, J., Griffin, W. L., Zhao, J., Tang, H., Ma, Q., & Lin, X. (2012). Geochemistry and geochronology of Carboniferous volcanic rocks in the eastern Junggar terrane, NW China: Implication for a tectonic transition. *Gondwana Research*, 22(3–4), 1009–1029. <https://doi.org/10.1016/j.gr.2012.01.004>
- Tang, G.-J., Wang, Q., Zhang, C., Wyman, D. A., Dan, W., Xia, X.-P., et al. (2017). Sr–Nd–Hf–O isotope geochemistry of the Ertaipei pluton, East Junggar, NWChina: Implications for development of a crustal-scale granitoid pluton and crustal growth. *Geochemistry, Geophysics, Geosystems*, 18(9), 3340–3358. <https://doi.org/10.1002/2017gc006998>
- Tao, H., Sun, S., Wang, Q., Yang, X., & Jiang, L. (2014). Petrography and geochemistry of lower carboniferous greywacke and mudstones in Northeast Junggar, China: Implications for provenance, source weathering, and tectonic setting. *Journal of Asian Earth Sciences*, 87, 11–25. <https://doi.org/10.1016/j.jseaes.2014.02.007>
- Tapponnier, P., Peltzer, G., Le Dain, A. Y., Armijo, R., & Cobbold, P. (1982). Propagating extrusion tectonics in Asia: New insights from simple experiments with plasticine. *Geology*, 10(12), 611. [https://doi.org/10.1130/0091-7613\(1982\)10](https://doi.org/10.1130/0091-7613(1982)10)
- Tapponnier, P., Zhiqin, X., Roger, F., Meyer, B., Arnaud, N., Wittlinger, G., & Jingsui, Y. (2001). Oblique stepwise rise and growth of the Tibet plateau. *Science*, 294(5547), 1671–1677. <https://doi.org/10.1126/science.105978>
- Tian, Z., Xiao, W., Shan, Y., Windley, B., Han, C., Zhang, J. e., & Song, D. (2013). Mega-fold interference patterns in the Beishan orogen (NW China) created by change in plate configuration during Permo–Triassic termination of the Altai. *Journal of Structural Geology*, 52, 119–135. <https://doi.org/10.1016/j.jsg.2013.03.016>
- Treagus, S. H. (1973). Buckling stability of a viscous single-layer system, oblique to the principal compression. *Tectonophysics*, 19(3), 271–289. [https://doi.org/10.1016/0040-1951\(73\)90022-X](https://doi.org/10.1016/0040-1951(73)90022-X)
- Vallée, M. A., Keating, P., Smith, R. S., & St-Hilaire, C. (2004). Estimating depth and model type using the continuous wavelet transform of magnetic data. *Geophysics*, 69(1), 191–199. <https://doi.org/10.1190/1.1649387>
- Van der Voo, R. (2004). Paleomagnetism, oroclines, and growth of the continental crust. *Geological Society of America Today*, 14(12), 4. [https://doi.org/10.1130/1052-5173\(2004\)014](https://doi.org/10.1130/1052-5173(2004)014)
- Verdusco, B., Fairhead, J. D., Green, C. M., & MacKenzie, C. (2004). New insights into magnetic derivatives for structural mapping. *The Leading Edge*, 23(2), 116–119. <https://doi.org/10.1190/1.1651454>
- Viola, G., & Mancktelow, N. S. (2005). From XY tracking to buckling: Axial plane cleavage fanning and folding during progressive deformation. *Journal of Structural Geology*, 27(3), 409–417. <https://doi.org/10.1016/j.jsg.2004.10.011>
- Wang, T., Jahn, B.-M., Kovach, V. P., Tong, Y., Hong, D.-W., & Han, B.-F. (2009). Nd–Sr isotopic mapping of the Chinese Altai and implications for continental growth in the Central Asian Orogenic Belt. *Lithos*, 110(1–4), 359–372. <https://doi.org/10.1016/j.lithos.2009.02.001>
- Wang, T., Tong, Y., Huang, H., Zhang, H., Guo, L., Li, Z., et al. (2023). Granitic record of the assembly of the Asian continent. *Earth-Science Reviews*, 237, 104298. <https://doi.org/10.1016/j.earscirev.2022.104298>
- Wang, Z., Sun, S., Li, J., Hou, Q., Qin, K., Xiao, W., & Hao, J. (2003). Paleozoic tectonic evolution of the northern Xinjiang, China: Geochemical and geochronological constraints from the ophiolites. *Tectonics*, 22(2). <https://doi.org/10.1029/2002tc001396>
- Wilhem, C., Windley, B. F., & Stampfli, G. M. (2012). The Altai of central Asia: A tectonic and evolutionary innovative review. *Earth-Science Reviews*, 113(3–4), 303–341. <https://doi.org/10.1016/j.earscirev.2012.04.001>

- Windley, B. F., Alexiev, D., Xiao, W. J., Kroner, A., & Badarch, G. (2007). Tectonic models for accretion of the central Asian orogenic belt. *Journal of the Geological Society*, *164*(1), 31–47. <https://doi.org/10.1144/0016-76492006-022>
- Windley, B. F., Kroner, A., Guo, J. H., Qu, G. S., Li, Y. Y., & Zhang, C. (2002). Neoproterozoic to Paleozoic geology of the Altai Orogen, NW China: New zircon age data and tectonic evolution. *The Journal of Geology*, *110*(6), 719–737. <https://doi.org/10.1086/342866>
- Xiao, W., Han, C., Yuan, C., Sun, M., Lin, S., Chen, H., et al. (2008). Middle Cambrian to Permian subduction-related accretionary orogenesis of northern Xinjiang, NW China: Implications for the tectonic evolution of central Asia. *Journal of Asian Earth Sciences*, *32*(2–4), 102–117. <https://doi.org/10.1016/j.jseae.2007.10.008>
- Xiao, W., Huang, B., Han, C., Sun, S., & Li, J. (2010). A review of the western part of the Altaids: A key to understanding the architecture of accretionary orogens. *Gondwana Research*, *18*(2–3), 253–273. <https://doi.org/10.1016/j.gr.2010.01.007>
- Xiao, W., Windley, B. F., Badarch, G., Sun, S., Li, J., Qin, K., & Wang, Z. (2004). Palaeozoic accretionary and convergent tectonics of the southern Altaids: Implications for the growth of central Asia. *Journal of the Geological Society*, *161*(3), 339–342. <https://doi.org/10.1144/0016-764903-165>
- Xiao, W., Windley, B. F., Han, C., Liu, W., Wan, B., Zhang, J. e., et al. (2018). Late Paleozoic to early Triassic multiple roll-back and oroclinal bending of the Mongolia collage in Central Asia. *Earth-Science Reviews*, *186*, 94–128. <https://doi.org/10.1016/j.earscirev.2017.09.020>
- Xiao, W., Windley, B. F., Sun, S., Li, J., Huang, B., Han, C., et al. (2015). A Tale of amalgamation of three Permo-Triassic collage systems in central Asia: Oroclines, sutures, and terminal accretion. *Annual Review of Earth and Planetary Sciences*, *43*(1), 477–507. <https://doi.org/10.1146/annurev-earth-060614-105254>
- Xiao, W. J., Windley, B. F., Yuan, C., Sun, M., Han, C. M., Lin, S. F., et al. (2009). Paleozoic multiple subduction-accretion processes of the southern Altaids. *American Journal of Science*, *309*(3), 221–270. <https://doi.org/10.2475/03.2009.02>
- Xu, K., Jiang, Y., Wang, S., Shu, T., Li, Z.-Y., Collett, S., et al. (2021). Multi-phase tectonothermal evolution in the SE Chinese Altai, central Asia: Structures, U-Pb monazite ages and tectonic implications. *Lithos*, *392–393*, 392–393. <https://doi.org/10.1016/j.lithos.2021.106148>
- Xu, Q., Zhao, L., Niu, B., Zheng, R., Yang, Y., & Liu, J. (2020). Early Paleozoic arc magmatism in the Kalamaili orogenic belt, northern Xinjiang, NW China: Implications for the tectonic evolution of the East Junggar terrane. *Journal of Asian Earth Sciences*, *194*, 104072. <https://doi.org/10.1016/j.jseae.2019.104072>
- Xu, X., Jiang, N., Li, X.-H., Qu, X., Yang, Y.-H., Mao, Q., et al. (2013). Tectonic evolution of the East Junggar terrane: Evidence from the Taheir tectonic window, Xinjiang, China. *Gondwana Research*, *24*(2), 578–600. <https://doi.org/10.1016/j.gr.2012.11.007>
- Yang, F., Mao, J., Pirajno, F., Yan, S., Liu, G., Zhou, G., et al. (2012). A review of the geological characteristics and geodynamic setting of Late Paleozoic porphyry copper deposits in the Junggar region, Xinjiang Uygur Autonomous Region, Northwest China. *Journal of Asian Earth Sciences*, *49*, 80–98. <https://doi.org/10.1016/j.jseae.2011.11.024>
- Yang, G., Li, Y., Santosh, M., Yang, B., Zhang, B., & Tong, L. (2013). Geochronology and geochemistry of basalts from the Karamay ophiolitic melange in West Junggar (NW China): Implications for Devonian-Carboniferous intra-oceanic accretionary tectonics of the southern Altaids. *Geological Society of America Bulletin*, *125*(3–4), 401–419. <https://doi.org/10.1130/b30650.1>
- Ye, X.-T., Zhang, C.-L., Zou, H.-B., Yao, C.-Y., & Dong, Y.-G. (2016). Age and geochemistry of the Zhaheba ophiolite complex in eastern Junggar of the central Asian orogenic belt (CAOB): Implications for the accretion process of the Junggar terrane. *Geological Magazine*, *154*(3), 419–440. <https://doi.org/10.1017/s0016756816000042>
- Zhang, C.-L., Santosh, M., Zou, H.-B., Xu, Y.-G., Zhou, G., Dong, Y.-G., et al. (2012). Revisiting the “Irish tectonic belt”: Implications for the Paleozoic tectonic evolution of the Altai orogen. *Journal of Asian Earth Sciences*, *52*, 117–133. <https://doi.org/10.1016/j.jseae.2012.02.016>
- Zhang, J., Xiao, W., Luo, J., Chen, Y., Windley, B. F., Song, D., et al. (2018). Collision of the Tacheng block with the Mayile-Barleik-Tangbale accretionary complex in western Junggar, NW China: Implication for early-middle Paleozoic architecture of the western Altaids. *Journal of Asian Earth Sciences*, *159*, 259–278. <https://doi.org/10.1016/j.jseae.2017.03.023>
- Zhang, M., Wang, G., Zhang, X., Liao, Q. a., Wang, W., Guo, R., & Zhang, P. (2021). Reconstruction of the Silurian to Devonian stratigraphic succession along the northeastern margin of the Junggar block, Xinjiang, NW China, and its tectono-paleogeographic implications for the southwestern central Asian orogenic belt. *Sedimentary Geology*, *411*, 105780. <https://doi.org/10.1016/j.sedgeo.2020.105780>
- Zhang, P., Wang, G., Polat, A., Shen, T., Chen, Y., Zhu, C., & Wu, G. (2018). Geochemistry of mafic rocks and cherts in the Darbut and Karamay ophiolitic mélanges in West Junggar, northwestern China: Evidence for a Late Silurian to Devonian back-arc basin system. *Tectonophysics*, *745*, 395–411. <https://doi.org/10.1016/j.tecto.2018.08.018>
- Zhang, P., Wang, G., Polat, A., Zhu, C., Shen, T., Chen, Y., et al. (2018). Emplacement of the ophiolitic mélanges in the west Karamay area: Implications for the Late Paleozoic tectonic evolution of West Junggar, northwestern China. *Tectonophysics*, *747–748*, 259–280. <https://doi.org/10.1016/j.tecto.2018.08.019>
- Zhang, Y., & Guo, Z. (2010). New constraints on formation ages of ophiolites in the northern Junggar and comparative study on their connection. *Acta Petrologica Sinica*, *26*, 421–430. (In Chinese with the English abstract).
- Zhang, Y., Pe-Piper, G., Piper, D. J. W., & Guo, Z. (2013). Early Carboniferous collision of the Kalamaili orogenic belt, North Xinjiang, and its implications: Evidence from molasse deposits. *Geological Society of America Bulletin*, *125*(5–6), 932–944. <https://doi.org/10.1130/b30779.1>
- Zhang, Z., Zhou, G., Kusky, T. M., Yan, S., Chen, B., & Zhao, L. (2009). Late Paleozoic volcanic record of the Eastern Junggar terrane, Xinjiang, Northwestern China: Major and trace element characteristics, Sr–Nd isotopic systematics and implications for tectonic evolution. *Gondwana Research*, *16*(2), 201–215. <https://doi.org/10.1016/j.gr.2009.03.004>
- Zhou, J.-B., Wilde, S. A., Zhao, G.-C., & Han, J. (2018). Nature and assembly of microcontinental blocks within the Paleo-Asian Ocean. *Earth-Science Reviews*, *186*, 76–93. <https://doi.org/10.1016/j.earscirev.2017.01.012>

References From the Supporting Information

- Li, X., Tang, G., Gong, B., Yang, Y., Hou, K., Hu, Z., et al. (2013). Qinghu zircon: A working reference for microbeam analysis of U-Pb age and Hf and O isotopes. *Chinese Science Bulletin*, *58*(36), 4647–4654. <https://doi.org/10.1007/s11434-013-5932-x>
- Ludwig, K. R. (2012). Isoplot/ex Version 4.15. A geochronological Toolkit for Microsoft Excel [Software]. *Berkeley Geochronology Center Special Publication*, *5*, 75. <https://www.bgc.org/isoplot>
- Pearce, N. J. G., Perkins, W. T., Westgate, J. A., Gorton, M. P., Jackson, S. E., Neal, C. R., & Chenery, S. P. (1997). A compilation of new and published major and trace element data for NIST SRM 610 and NIST SRM 612 glass reference materials. *Geostandards and Geoanalytical Research*, *21*(1), 115–144. <https://doi.org/10.1111/j.1751-908X.1997.tb00538.x>
- Sláma, J., Košler, J., Condon, D. J., Crowley, J. L., Gerdes, A., Hanchar, J. M., et al. (2008). Plešovice zircon—A new natural reference material for U–Pb and Hf isotopic microanalysis. *Chemical Geology*, *249*(1–2), 1–35. <https://doi.org/10.1016/j.chemgeo.2007.11.005>